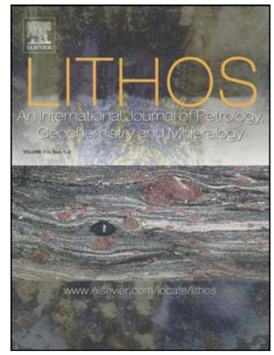

Accepted Manuscript

Geochronology of accessory allanite and monazite in the Barrovian metamorphic sequence of the Central Alps, Switzerland

Kate R. Boston, Daniela Rubatto, Jörg Hermann, Martin Engi, Yuri Amelin

PII: S0024-4937(17)30236-0
DOI: doi:10.1016/j.lithos.2017.06.025
Reference: LITHOS 4357

To appear in: *LITHOS*

Received date: 20 February 2017
Accepted date: 23 June 2017

Geochronology of accessory allanite and monazite in the Barrovian metamorphic sequence of the Central Alps, Switzerland

Kate R. Boston[1], Daniela Rubatto[1,2,3*], Jörg Hermann[1,2], Martin Engi[2] and Yuri Amelin[1]

1) Research School of Earth Sciences, Australian National University, Canberra, ACT 2601 Australia

2) Institute of Geological Sciences, University of Bern, Baltzerstrasse 1-3, 3012 Bern, Switzerland

3) Institut de Sciences de la Terre, University of Lausanne, Bâtiment Géopolis, 1015 Lausanne, Switzerland

*Corresponding author: daniela.rubatto@geo.unibe.ch

Abstract

The formation of accessory allanite, monazite and rutile in amphibolite facies rocks across the Barrovian sequence of the Central Alps (Switzerland) was investigated with a combination of petrography and geochemistry and related to the known structural and metamorphic evolution of the Lepontine dome. For each of these minerals a specific approach was adopted for geochronology, taking into account internal zoning and U-Th-Pb systematics. In-situ U-Th-Pb dating of allanite and monazite by ion microprobe revealed systematic trends for the ages of main deformation and temperature in the Lepontine dome. Isotope dilution TIMS dating of rutile returns dates in line with this picture, but is complicated by inheritance of pre-Alpine rutile and possible Pb loss during Alpine metamorphism.

Allanite is generally a prograde mineral that is aligned along the main foliation of the samples and found also as inclusions in garnet. Prograde allanite formation is further documented by rutile inclusions with formation temperatures significantly lower than the maximum T recorded by the rock mineral assemblage. Allanite ages vary from 31.3 ± 1.1 Ma in orthogneisses in the East to 31.7 ± 1.1 Ma for a Bündnerschiefer and 28.5 ± 1.3 Ma for a metaquartzite in the central area, to 26.8 ± 1.1 Ma in the western part of the Lepontine dome. These ages are interpreted to date the main deformation events (nappe stacking and isoclinal deformation of the nappe stack), close to peak pressure conditions.

The timing of the thermal peak in the Lepontine dome is recorded in monazite that grew at the expense of allanite and after a main episode of garnet growth at temperatures of ~620°C. Monazite in the central area yields an age of 22.0 ± 0.3 Ma, which is indistinguishable from the age of 21.7 ± 0.4 Ma from a metapelite in the western part of the Lepontine dome. In the central area some of the classical kyanite-staurolite-garnet schists directly underlying the metamorphosed Mesozoic sediments contain monazite that records only a pre-Alpine, Variscan metamorphic event of upper greenschist to lower amphibolite facies conditions dated at ~330 Ma.

The new age data provide evidence that nappe stacking at prograde amphibolite facies conditions and refolding of the nappe stack occurred between 32 and 27 Ma, only a few million years after eclogite facies metamorphism in the Adula-Cima Lunga unit. Amphibolite facies metamorphism lasted for about 10 My to ~22 Ma, allowing for multiple ductile deformation and recrystallization events. The long lasting amphibolite facies metamorphism requires fast cooling between 20 and 15 Ma in the Central Alps. This fast cooling was not related to an increase in sedimentation rates in the foreland basins, suggesting that tectonic exhumation was responsible for termination of amphibolite facies metamorphism in the Lepontine dome.

Keywords

Accessory minerals; Barrovian metamorphism; Central Alps; ion-microprobe; metamorphic petrology; SHRIMP; U-Pb dating.

1. Introduction

Well-constrained geochronology is essential for understanding metamorphic processes that occur during orogenesis. Not only are ages of metamorphic events important for establishing and correlating the timing of orogen-scale processes but equally important is the rate at which these processes occur. Finding evidence of a prograde history, crucial for evaluating models of heat transfer during orogenesis, is often difficult because such evidence within a sample is usually obliterated by subsequent, higher-grade metamorphism. Therefore, geochronology of Barrovian metamorphic terranes is best achieved by combining different geochronometers that are reactive under different conditions and thus may preserve different stages of the P-T evolution. Allanite, monazite, and rutile (or titanate) are well-suited chronometers for medium grade terrains, where the more reliable geochronometer zircon, is commonly not reactive (e.g. Romer et al., 1996; Vonlanthen et al., 2012, see also a review in Rubatto, 2017).

At upper greenschist-facies conditions, allanite can replace detrital or low-grade metamorphic monazite; subsequently monazite crystallises at the expense of allanite at middle amphibolite-facies conditions (e.g. Smith and Barreiro, 1990; Finger et al., 1998; Wing et al., 2003; Janots et al., 2008; Kim et al., 2009). The reactions of monazite to allanite and allanite to monazite do not take place in all rock types and at the same conditions (Engi, 2017). The proposed variables controlling the reactions include bulk composition (Finger et al., 1998; Wing et al., 2003; Janots et al., 2008; Spear, 2010), fluid composition (Budzýn et al., 2010), the oxygen fugacity of the fluid (Janots et al., 2011), and pressure (Janots et al., 2007; Spear, 2010). The use of allanite as U-Th-Pb geochronometer is complicated by internal complexity (zoning) and typically high concentration of initial Pb incorporated into the mineral during crystallisation (e.g. Romer and Siegesmund, 2003). The problem of initial Pb in allanite has been addressed by Gregory et al. (2007) and Smye et al. (2014). It has been demonstrated that regression in a Tera-Wasserburg diagram or the Th-isochron technique (Gregory et al., 2007) eliminates the need to assume the isotopic composition of initial Pb and allows determination of geologically significant ages even for allanite with high amounts of initial Pb (Janots and Rubatto, 2014). Additional issues with allanite are the relative mobility of Th and U resulting in Th-U fractionation (Smye et al., 2014). Monazite and allanite potentially incorporate excess of ^{206}Pb produced by the decay of ^{230}Th, which can compromise the $^{206}Pb/^{238}U$ ratios. Therefore, calculation of isotopic ages and their interpretation for these minerals demands special attention to these complications.

At amphibolite facies conditions, the stable Ti-bearing phase can be rutile, titanite or ilmenite; their relative stability is controlled by pressure, temperature and bulk rock composition. Rutile has the advantage that it generally does not incorporate initial Pb at formation, but can contain very low U concentrations that render precise measurement of radiogenic isotopic ratios difficult (Kooijman et al., 2010, Warren et al., 2012; Smye et al., 2014).

Petrography is required to link the growth of accessory minerals to metamorphic structures and major mineral phases (Janots et al., 2008; Janots et al., 2011; Regis et al., 2014). The relative timing of monazite and allanite can also be linked to major phases such as garnet through trace element distributions (e.g. Foster et al., 2002; Hermann and Rubatto 2003; Buick et al., 2006). Both allanite and monazite commonly preserve multiple growth zones, and individual growth zones can be analysed by *in situ* techniques. Minerals that yield ages from more than one growth zone can be used for inferring metamorphic rates, provided that metamorphic conditions can be established for each growth zone (e.g. Hermann and Rubatto, 2003; Janots et al., 2009; Pollington and Baxter, 2010; Rubatto et al., 2011; Janots and Rubatto, 2014; Regis et al., 2014).

The various challenges related to monazite, allanite and rutile geochronology (e.g. multiple growth zones, common and inherited initial Pb, low U content, different reactivity, etc...) may reduce accuracy and precision of single age determinations. A mineral-specific approach to U-Th-Pb analysis and data treatment is required because of the different U-Th-Pb systematics in monazite, allanite and rutile: bulk *versus* micro-sampling methods according to internal zoning, U-Pb or Th-Pb system and different approaches to corrections for initial Pb. Dating of multiple mineral zones in the same rock and comparison of ages from diverse lithologies, both locally and over regional scale will also increase reliability of the ages.

We apply the multi-mineral dating approach to the classical Barrovian, middle grade sequence of the Lepontine Central Alps, Switzerland. This metamorphic sequence has been the subject of half a century of study, following the reaction boundary maps of Niggli and Niggli (1965). Geochronology studies in the area date back four decades to the pioneering work of Hunziker, Jäger, Köppel and Steiger (Hunziker, 1969; Jäger, 1973; Köppel and Grünenfelder, 1975; Deutsch and Steiger, 1985; Steck and Hunziker, 1994). Despite the long history of geochronology there remain significant uncertainties and debates on the timing and duration of Barrovian metamorphism. The lack of consensus is mainly due to uncertainty regarding the extent to which dated micas and amphibole represent inherited, formation or cooling ages considering the metamorphic grade and complex metamorphic history preserved the rocks in the Central Alps (parts of which span two or more orogenic cycles). The present study is focused on areas between the Northern and Southern Steep Belts, encompassing almost the entire East-to-West breadth of the Lepontine dome.

2. Geological background

The Lepontine dome of the Central Alps extends between the Northern and Southern Steep Belts (NSB and SSB respectively), the Simplon line in the west, and Bergell area in the east (Fig. 1). The nappe stack in the dome comprises polymetamorphic basement units and Mesozoic sedimentary cover units; both are overprinted by a Barrovian sequence that reached maximum temperatures just north of the Insubric line (e.g. Frey et al., 1974; Frey et al., 1980; Trommsdorff, 1980; Engi et al., 1995; Todd and Engi, 1997). Concentric isograds and isotherms document an increase in metamorphic grade from lower-amphibolite facies in the Northern Steep Belt (NSB) to upper-amphibolite facies with partial melting in the Southern Steep Belt (SSB, Fig. 1b).

This study investigates metasediments from the cover sequences as well as basement rocks (Table 1). The Permo-Mesozoic sedimentary units were deposited on the subsiding European continental margin during the extensional phase in between the Variscan and Alpine orogenies (Grujic and Mancktelow, 1996; Berger et al., 2005; Garofalo, 2012).   During Alpine metamorphism the peak temperature was reached after nappe formation and emplacement, as mineral zone boundaries and isotherms discordantly crosscut tectonic boundaries (Fig. 1b; Niggli and Niggli, 1965; Frey et al., 1980; Engi et al., 1995; Todd and Engi, 1997). In the southern portion of the Lepontine dome, Barrovian metamorphism is considered to be syn- to post-kinematic with refolding of the established nappe pile and exhumation of some high-pressure rocks (Frey et al., 1980; Nagel et al., 2002; Brouwer et al., 2004; Brouwer et al., 2005; Berger et al., 2005; Rütti et al., 2008; Berger et al., 2011). In the northern part of the Lepontine, Barrovian metamorphism probably reached T_{max} conditions after most of the major thrusts ceased to operate (Berger et al., 2005; Wiederkehr et al., 2008; Janots et al., 2009; Wiederkehr et al., 2009; Berger et al., 2011). However, Wiederkehr et al. (2011) showed that near the NE-margin isotherms are steeply inclined, affected by late-orogenic km-scale folding, and may be displaced along a major nappe boundary (in the footwall of the Adula thrust sheet). In the study area, Barrovian metamorphic conditions reached temperatures of 550-650 °C and pressures of 7 kbar or less at peak temperature (Engi et al., 1995; Todd and Engi, 1997).

The age of Barrovian metamorphism in the Central Alps is the subject of ongoing debate. Pioneering studies on mica geochronology (K-Ar, Rb-Sr) from outside the Lepontine dome, where peak metamorphic temperatures did not exceed the assumed closure temperature of the dated minerals, led to a long dominating view that placed peak Barrovian metamorphic conditions at 38-40 Ma (Jäger, 1973; Steck and Hunziker, 1994). On the other hand, K-Ar dating of amphiboles across the northern part of the Lepontine dome returned much younger ages of 32-23 Ma that were interpreted as formation ages (Deutsch and Steiger, 1985). Such younger metamorphic ages had been previously documented in monazite from the centre of the Lepontine dome (Köppel and Grünenfelder, 1975) but no relation of monazite age to metamorphic assemblage was shown. More recent work emphasised crystallisation ages of accessory minerals, and this now points to a younger age (17-32 Ma) for Barrovian metamorphism and an age gradient across the belt (e.g. Janots et al., 2009; Rubatto et al., 2009; Berger et al., 2011). *In situ* zircon and allanite ages for protracted melting in migmatites from the SSB span from ~ 32 to 22 Ma, indicating that temperatures were high in the southernmost part of the Lepontine dome up to 22 Ma (Rubatto et al., 2009; Gregory et al., 2012). Similarly, studies on rocks in the northern limits of the Lepontine dome have established an 18-19 Ma age for T_{max} (Janots et al., 2009). Based on U-Pb in monazite, this young age for T_{max} is supported by 15-18 Ma Ar-Ar ages in white mica in rocks in the north-east of the Lepontine Dome (Wiederkehr et al., 2009) and in the Lucomagno area (Allaz et al., 2011).

The modern geochronology studies have mainly focussed on areas in the Southern- and Northern Steep Belts (Gebauer 1996; Romer et al., 1996; Janots et al., 2009; Rubatto et al., 2009; Wiederkehr et al., 2009), and data from the central part of the dome remain scarce. In this area, zircon was largely unreactive under medium grade metamorphic conditions and indeed our attempt to date the rare and thin zircon metamorphic overgrowths only returned scattered dates that do not represent significant ages. Systems utilising micas (e.g. K-Ar, Ar-Ar, Rb-Sr) have been interpreted to largely record cooling, retrograde reactions, or they retain pre-Alpine relics (e.g. Jäger, 1973; Hurford 1986; Janots et al., 2009; Allaz et al., 2011).

3. Sample description and petrography of accessory minerals

Sample locations of this contribution are from as far north as Campolungo (south-east of Airolo, Fig. 1b); the Western-most sample is from Croveo, north of Domodossola. Eastern-most samples are from the Forcola area, ~ 75 km east of Croveo and west of Chiavenna. The geographical spread of samples across this central part of the Lepontine dome provides ages that can reconcile the data sets of the NSB and SSB.

Our samples in the central Lepontine dome record sub-solidus amphibolite-facies conditions during Barrovian metamorphism. For the same area, Todd and Engi (1997) reported, T_{max} varying from 550°C in the lower grade rocks, to 620°C in the highest-grade samples. Pressures estimated for equilibration of the rocks (i.e. at maximum T) vary between 5 kbar in the eastern-most samples and < 6.5 kbar in samples in the central to western part of the study area (Todd and Engi, 1997). An overview of sample locations, mineral assemblages and geochronology is presented in Table 1. Details of the mineral textures and compositions are presented in the electronic Appendix. Important textural relationships regarding key major and accessory minerals are shown in Fig. 2. Bulk rock analyses of the samples – excluding sample Sp9312, which has distinct compositional layering – are given in Table A1.

4. Mineral composition

4.1. Garnet

Croveo schist (Ma9330) garnet grains have core-rim compositional zoning (Fig. 4a, Table A2). Garnet cores are rich in Mn and Ca (MnO = 5.8 wt%; CaO = 8.1 wt%), which decrease towards the rims. Fe and Mg have the opposite trend, with lowest concentrations in the core (FeO = 27 wt%; MgO = 0.85 wt%), increasing outwards. The HREE and Y concentrations are highest in the core (Y = 370 ppm, Yb = 96 ppm) and decrease dramatically before increasing again towards the outer rim. The increase in HREE+Y in the outer rim is taken to indicate garnet resorption. HREE patterns are steepest in the core (Dy_N/Lu_N = 0.03) and become flatter outwards ($Dy_N/Lu_N \leq 1.4$). Garnet outer rims are characterised by a flat to negative HREE slope ($Dy_N/Lu_N > 2$, Fig. 4b). Garnet cores and rims have a weak negative Eu anomaly of = 0.4-0.7.

Garnet grains in CLB-3 Campolungo calcschist show a simple core-to-rim zoning in the inner part of the garnet (Grt I) with some subtle complexity in the grain rim, (Grt II, Fig. 4c). CLB-3 Grt I cores are rich in Mn (MnO = 2.3 wt%) and poor in Mg (MgO = 1.6

wt%) compared to Grt II (MnO = 0.4 wt%; MgO = 2.4 wt%). Garnet grains in this sample are remarkably low in REE (Fig. 4d, Table A2). LREE concentrations were often below the limit of detection (typically 0.002 ppm for Ce, 0.003 ppm for La), and only REE heavier than Eu were consistently above detection limits. HREE slopes are steep in Grt I cores (Dy_N/Lu_N = 0.008) and become gentler outwards (Dy_N/Lu_N = 0.15 near Grt II). Grt II is characterised by relative enrichment in some HREE, particularly Tb to Er.

Garnet in sample CLM-5 and 6 has a distinct core that is rich in inclusions of graphite. The inclusion-poor rim is separated from the core by an irregular annulus that cuts across the zoning of the core (Fig. 4e-f). The core is poor in MgO (1-4–2.5 wt%) and richer in CaO (0.7-2.6 wt%) and MnO (0.7-4.2 wt%) with respect to the rim (MgO = 3.0-3.5, CaO = 0.4, MnO = 0.13-0.4 wt%). The large core generally shows a decrease in these elements from the inner to the outer part, and additional Mn and Ca patchy zoning in CLM-5 or oscillatory zoning in CLM-6 (Fig. 4f). The core of CLM-6 garnet contains inclusions of chloritoid (X_{Mg}=0.14), rare staurolite (X_{Mg}=0.07), chlorite, quartz, ilmenite and rutile. The discordant rim is more homogeneous in composition with a slight increase in Mg outwards. Ilmenite, rutile, chlorite, quartz and rare chloritoid (X_{Mg}=0.19) inclusions have been observed. Staurolite in the matrix coexists with garnet rims and displays significantly higher X_{Mg}=0.21 than staurolite inclusions.

Alpe Sponda fels Sp9712 contains garnet with complex zoning in major and trace element composition. Because garnet grains are scarce in Sp9712, they were analysed as polished grains retrieved from the sample separate. Ca element maps of larger grains show an outward increase in Ca from the core (Grt I), before an abrupt drop in concentration in Grt II (Fig. 4g). A number of garnet grains show embayment to the Ca zoning. In these garnets, Fe shows a complementary trend to Ca, decreasing from the core before increasing in Grt II. The trace element zoning is best seen in HREE concentrations. Grt I cores display little zoning (Fig. 4g) and have a flat HREE pattern. Towards the rim of Grt I the HREE significantly decrease. Grt II is marked by an increase in HREE to higher levels than what is observed in Grt I cores, followed by a decrease towards the rims of Grt II.

One small (200 μm diameter) euhedral garnet grain with distinctive composition (Grt III) presents a relatively simple, bell-shaped zoning with cores enriched in Ca and Y, which decrease towards the rims. HREE are even more extremely enriched than in Grt II (Dy_N/Lu_N = 0.1-0.4, Fig. 4h) with greatest HREE enrichment occurring in the core. Y concentration is as high as 3 wt % in garnet cores and decreases to ~ 3500 ppm at the rim. Element maps of major and trace elements suggest that Grt II and Grt III formed at the same time, with the first one as overgrowth on pre-existing, partially resorbed cores and the latter as newly formed, small individual grains.

4.2. Allanite

Metasediments. The compositional zoning of allanite is similar in the metasediment samples from the western and central areas (Robiei Ba0901, Campolungo CLB-3 and Ma0901); they are considered here together. Allanite has three distinctive zones: a LREE-enriched core, a HREE-enriched mantle, and an epidote rim (Fig. 3a-d). Ba0901 has one additional allanite rim that is overgrown on epidote.

Robiei (Ba0901) LREE-allanite cores and rims have similar REE patterns (Fig. 5a) with a significant negative Eu anomaly (Eu/Eu* = 0.3-0.5 in cores and 0.2-0.5 in rims) and a similar HREE slope (Dy_N/Lu_N = 4.5 in cores and 5.5 in rims). Ba0901 allanite cores vary in Th from 4300 to 12000 ppm, U spans from 600 to 1500 ppm, and Th/U ratio varies from 2.8 to 12 (Table A4). Ba0901 LREE-allanite rims are similar in composition to cores of the same grains but differ in the abundance of HREE, which tend to be higher in the rims than cores. Th concentration is lower in rims (2000-8000 ppm) and U concentration is similar to cores (300-1700 ppm). Th/U ratios show little variation, with Th/U between 3.5 and 6.5 in allanite rims.

Samples from Campolungo (CLB-3 calcschist and Ma0901 quartzite, Fig. 3c-d) both lack the LREE-rich rim characteristic of the Robiei (Ba0901) allanite. The REE patterns of allanite cores in both samples have a significant negative Eu anomaly (Eu/Eu* = 0.6 in CLB-3 and 0.5 in Ma0901) and a steep HREE pattern (CLB-3 Dy_N/Lu_N = 7-17, Ma0901 Dy_N/Lu_N = 8-24; Fig. 5b-c). CLB-3 calcschist allanite cores have lower Th and U concentrations than in the quartzite (Ma0901). CLB-3 allanite cores contain 4300-7700 ppm Th and 100-400 ppm U; Ma0901 allanites contain 3300-18000 ppm Th and 400-1200 ppm U. Th/U ratios in CLB-3 are high and vary from 40 to 77; Th/U ratios in Ma0901 quartzite vary from 2.8 to 27.

Allanite mantles with a relative HREE- and U-enrichment (Fig. 5d) are only found in the metasediments. The HREE-allanite mantles are commonly thin and can have complex internal zoning, especially in the case of Ba0901 (Fig. 3a-b). In all allanite mantle zones, HREE concentrations decrease outwards. Campolungo allanites from both CLB-3 calcschist and Ma0901 quartzite have significant HREE enrichment in the mantle zone, and the HREE pattern has a concave down shape (Fig. 5b-c). HREE-allanites from all samples show a similarly weak negative Eu-anomaly (Eu/Eu* ≈ 0.75). U concentrations are much lower in the Campolungo calcschist than the quartzite (500 to 2300 ppm in CLB-3 calcschist and 1200 to 3500 ppm U in Ma0901); Th/U ratios in mantle allanite are much lower than in the cores for both samples (CLB-3 Th/U = 2-3; Ma0901 Th/U = 0.4-1).

Forcola orthogneiss. Despite the great variety of internal textures (Fig. 3f-h), allanites from orthogneiss samples (LEP0979, LEP0980, LEP0807) have similar trace element compositions. For all Forcola orthogneiss allanites, REE patterns have significant negative Eu anomalies (Eu/Eu* = 0.1-0.6, Fig. 5e-f) and a comparable HREE slope with Dy_N/Lu_N varying from 2 to 18. Th concentrations in orthogneiss allanites vary from 2000 to 20000 ppm; U concentration spans from 400 to 1200 ppm. The highest U concentrations occur in patchy allanite in sample LEP0807. Th/U ratios typically span between 4 and 31 in LEP0979 and LEP0807 allanites. LEP0980 regularly zoned allanite of Alpine age have a much lower Th/U ratio (Th/U = 0.2 to 12). The spectacularly zoned LEP0980 mosaic allanite have a trace element composition that is not distinctive and is within the range of the other Forcola orthogneiss allanites.

5.4. Monazite

REE composition of monazite is very similar in both samples (Croveo schist Ma9330, Alpe Sponda fels Sp9712) with a negative Eu anomaly (Eu/Eu* 0.5– 0.4) and a variable HREE slope (Fig. 5g, Table A5). U concentrations are similar in both samples (Ma9330 U = 3900-6300 ppm; Sp9712 U = 5400-6600 ppm) and Th concentrations are all but identical (Ma9330 Th = 21.8-34.1 %; Sp9712 Th = 25.2-34.7 %). Th/U ratios tend to be higher and more variable in Ma9330 monazites than in those from Sp9712 (Ma9330 Th/U = 5.0-7.9; Sp9712 Th/U = 4.6-6.3).

5. Rutile geothermometry

Selected rutiles were analysed for trace elements using LA ICP-MS (Table A3). The Zr content of rutile is a geothermometer (Ferry and Watson, 2007) that can provide crystallisation temperature estimates for the rutiles that are related to the growth of allanite cores (and hence their age) in Ma0901 quartzite and to the rutile bearing-paragenesis and/or ages in samples Ma9330, Ba0903A, CLB-3, CLB-4 and Sp9712. Following Ewing et al. (2013), the sources of uncertainty to be propagated onto Zr-in-rutile temperature estimates are the effect of analytical uncertainty of Zr measurement and uncertainty inherent in the calibration (~3 % for 500 °C, Ferry and Watson, 2007). The Zr analytical error was conservatively estimated to be ± 15 %, which corresponds to an error of ± 10-15 °C for the 500-650 °C temperature range and combined with the internal error of the calibration of Ferry and Watson (2007) it gives a total uncertainty of ± 20 °C for these samples.

Rutile from sample Ma9330, the western-most sample, returns a Zr-in-rutile temperature of ~ 565 °C (Zr = 100 ppm), clearly lower than T_{max} of 620 °C from Todd and Engi (1997). Ba0903A is of significantly lower grade than Ma9330 (T_{max} for this area is 575 °C, Todd and Engi, 1997) and the range of Zr concentrations in rutile from 100 to 166 ppm, corresponds to 565-595 °C. Samples CLB-3, CLB-4 and Ma0901 are all from the same locality and return Zr-in-rutile temperature estimates of ~ 565 °C, 625 °C and 580 °C, respectively (Zr = 100, 240 and 130 ppm, respectively). Sp9712 is the eastern-most rutile-bearing sample and returns a Zr-in-rutile temperature estimate of 550 °C (Zr = 85 ppm), which is again below the T_{max} expected for this area according to Todd and Engi (1997).

6. Geochronology

Depending on the assemblages of the investigated samples, monazite, allanite or rutile were dated. These minerals have different Th-U contents (rutile is virtually Th free and contains only 0.3 to 20 ppm U, monazite has Th/U of 5–10 and Alpine allanite has

Th/U of 2–80) and can variably incorporate initial Pb. Additionally, rutile shows no evident internal zoning, monazite shows limited evidence of internal zoning, whereas allanite is strongly zoned in both composition and age. Because of these inherent differences, geochronology of these minerals followed different approaches to achieve best age accuracy and precision.

Rutile was dated by ID-TIMS because of its low U content and the lack of intragrain zoning. Due to low U content, the measured Pb composition has a low radiogenic component and a significant proportion of initial Pb (Supplementary Table A8). Because these are multigrain fractions from different samples, with apparent different age they cannot be used for an isochron calculation and the best way to determine the initial Pb composition for each aliquot was to measure the composition of low-U-feldspar (Table A8b).

In the investigated samples, allanite is rich in Th and U, and both systems are strongly contaminated by initial Pb. The Th-Pb system in these samples is relatively more radiogenic than U-Pb (Supplementary Table A7) and thus it was preferred for age determination. Measuring the Pb composition of feldspar is not a rigorous approach to estimate the initial Pb composition for allanite in these samples because of the zoning complexity, the presence of different age populations, and the possibility of inherited initial Pb from precursor monazite (e.g. Romer and Rötzler, 2011). A better approach is to calculate Th-isochrons according to the methods of Gregory et al. (2007; $^{208}Pb/^{206}Pb_c$ versus $^{232}Th/^{206}Pb_c$ where $^{206}Pb_c$ is initial Pb only) for multiple analyses of the same domain in each sample. In this approach the assumption on common Pb composition (adopted to be the model composition of Stacey and Kramers 1975) has only marginal bearings on the calculation of the $^{206}Pb_c$ (see Gregory et al., 2007; Janots and Rubatto, 2014).

In monazite, unlike allanite, the initial Pb incorporation is low (mostly <3%) and thus the assumption on the common Pb composition has no bearing on the age within uncertainty. The U-Pb system was preferred to the Th-Pb system because of analytical setup (see methods).

6.1. Western Samples: Croveo (Ma9330) and Robiei (Ba0901)

Alpine ages are summarised in Fig. 6 and data are presented in Tables A5-A7. Monazite is the only accessory phase dated in the western-most sample Ma9330. The monazites are unzoned in BSE images and return a $^{206}Pb/^{238}U$ age of 21.7 ± 0.4 Ma (95 % confidence for all average ages, Fig. 7b) that is within error of the monazite age from central sample Sp9712 (see below).

Accessory allanite was dated in the Robiei sample Ba0901. Pre-Alpine igneous allanite relics returned dates that span from 397 to 187 Ma, a spread that may indicate alteration or partial resetting of the ^{232}Th-^{208}Pb isotopic system. Metamorphic allanite cores return an isochron age of 26.8 ± 2.3 Ma (MSWD = 2.0, n = 9/10; Fig. 8a). The scatter in the data is likely to be due to some minimal overlap of the SHRIMP analysis spot onto the surrounding growth zones, because of the small size of the cores. Allanite rim analyses define an isochron age of 19.7 ± 1.3 Ma (MSWD = 0.77, n = 11/12; Fig. 8b).

Rutile from Ba0903A calcschist returns a range of dates for different fractions that scatter from 21 to 27 Ma (Table A8). The oldest rutile date is from fraction A45 40, at 27.4 ± 1.7 Ma, which is similar to that of allanite cores from the same locality (Ba0901). Two fractions of orange grain fragments returned dates of 21.5 ± 2.5 Ma and 26.1 ±2.2 Ma.

6.2. Central samples: Campolungo (CLM-5, CLM-6, CLB-3, CLB-4, Ma0901) and Alpe Sponda (Sp9712)

Ages from allanite and monazite were extracted from the central samples (Fig. 6). Monazite in sample CLM-5 and 6 is pre-Alpine in age despite being aligned along the main foliation. They have weak internal zoning with sector and flame texture. Both samples returned a majority of dates between 322 and 339 ± 4 Ma (1σ) that define average ages of 331 ± 4 Ma and 326 ± 4, respectively (Fig. 7a). In both samples a few analyses show scattering towards younger dates that likely reflect Pb disturbance during Alpine overprint.

Allanite from CLB-3 calcschist returns an isochron age of 31.7 ± 1.1 Ma (MSWD = 1.5, n = 15/17, Fig. 8c), which is older than Ma0901 allanite cores from the same locality (28.5 ± 1.3 Ma, MSWD = 0.60, n = 27/29, Fig. 8d). Notably, for both samples, the weighted means of the most significant cluster of single spot dates – corrected for Pb_c using the model common Pb composition of Stacey and Kramers (1975) – are within error of the isochron ages (CLB-3 mean age 31.8 ± 0.9 Ma, MSWD = 1.7, N 10; Ma0901 29.6 ± 0.5 Ma, MSWD = 1.2, N 16). However, for the reasons given by Gregory et al. (2007) and Janots and Rubatto (2014), the isochron ages are deemed more reliable and are used in the discussion. Ma0901 HREE-rich allanite mantles are large enough to be analysed by SHRIMP but contained prohibitively high $f208$ (> 90%) and the data do not form a reliable isochron, preventing a reliable age calculation.

Rutile dates from one Campolungo sample (CLB-4) span from 19 to 25 Ma (Table A8). Like Ba0903A rutiles, the fractions comprising dark-coloured and larger grains and fragments tend to be older (~ 24 Ma, 4 fractions; Table A8) than the lighter honey-coloured rutile grains (~ 21 Ma, 3 fractions).

Sp9712 monazites return a $^{206}Pb/^{238}U$ age of 22.0 ± 0.3 Ma (Fig. 7c; Table A6). Monazites are subtly heterogeneous in BSE images (Fig. 7c), but there is no correlation between zoning and age. The monazite age is within error of the monazite age from Ma9330. Two groups of dates were obtained from Sp9712 rutiles (Table A8). Dark red-brown rutiles returned older dates between 52 and 57 Ma; the apparently younger rutiles are orange and light honey-coloured grains at 33.45 ± 0.37 Ma (Table A8).

6.3. Eastern samples: Forcola Orthogneiss (LEP0979, LEP0980, LEP0807)

Two orthogneiss samples contain metamorphic allanite that return acceptable isochron ages (MSWD < 2). Subgrain cores from LEP0980 mosaic allanites return an isochron age of 31.3 ± 1.1 Ma (MSWD = 1.1, n = 16/16; Fig. 8e); allanite from LEP0807, the structurally shallowest Forcola sample, return an isochron age of 27.4 ± 0.6 Ma (MSWD = 1.9, n = 17/21; Fig. 8f).

Allanites that did not form meaningful isochrons (MSWD > 2) are LEP0979 allanites, regularly zoned LEP0980 allanites, and subgrain rims of LEP0980 mosaic allanite. For these sample ^{207}Pb-corrected single spot dates are presented in Table A7, and in all cases they show a range of several Ma, suggesting the isotopic systematic was disturbed or individual grains contained variable initial Pb. Such dates are not taken individually to constrain significant geological events.

7. Discussion

7.1. Reliability of ages

At low to medium metamorphic grade allanite and monazite can replace each other (Janots et al., 2008; Janots et al., 2009) or grow from previous magmatic allanite or monazite with possible incorporation of radiogenic Pb from the precursor phase (e.g.

Romer and Siegesmund, 2003; Romer and Rötzler, 2011). This inheritance has bearings on initial Pb composition and thus age calculation. For the analysed monazite the fraction of initial Pb is small enough to make this problem minimal. Any incorporation of inherited radiogenic Pb would imply a lower $^{207}Pb/^{206}Pb$ ratio of the initial Pb and mildly shift the calculated age to younger values. Notably any excess ^{206}Pb may lead to a shift to older ages (see below).

For allanite the presence of inherited radiogenic and common Pb is a more serious problem, but the Th-isochron calculation is largely independent from the initial Pb composition, which is only used to determine the fraction of initial ^{206}Pb (see Gregory et al., 2007). Additionally, in the sample investigated, single spot ages calculated assuming a secular Pb composition (Stacey and Kramers, 1975) are mostly close to the Th-isochron age, indicating that initial Pb incorporated at growth was generally non radiogenic. This observation also limits the possibility of a shift in the age due to chemical inheritance as described by Romer and Siegesmund (2003) and Romer and Rötzler (2011). For allanite domains that do not yield an isochron age, the range of single spot dates are not given a geological significance as they may be affected by Pb inheritance. This is likely the case for the mosaic allanite in orthogneiss LEP0980 (Fig. 3h), where the subsolidus reaction that recrystallized the pre-Alpine allanite into the mosaic Alpine allanite was likely a closed system reaction and thus the Pb did not equilibrate.

Excess ^{206}Pb due to the incorporation of ^{230}Th at growth is another issue to consider in dating Th-rich minerals. Unlike magmatic systems, in metamorphic rocks a correction for excess ^{206}Pb based on the Th/U of the system is not possible because of changing reactive bulk during metamorphism. While this does not affect the Th-Pb system used for allanite dating, it can produce apparently older $^{206}Pb/^{238}U$ ages for monazite. Unlike magmatic monazite grown from a melt, excess ^{206}Pb in metamorphic monazite has been rarely reported (see Rubatto et al., 2013; Wang et al., 2015). Monazite analyses in this study are concordant within analytical uncertainty and this indicates that any excess ^{206}Pb is less than the analytical uncertainty of the $^{206}Pb/^{238}U$ ratio of single analyses, that is 0.6–1.5% relative for Variscan monazites and 2–4% in Alpine monazite.

In all analysed samples, rutile U contents are low, (mostly below 15 ppm with the exclusion of sample CLB where U content is 26-36 ppm, Table A3) and the proportion of initial Pb is thus high, with molar fraction of non-radiogenic ^{206}Pb between 0.75 and 0.98 (Table A8). To attempt non-radiogenic Pb correction, the Pb composition of K-feldspar was measured in sample CLB4 and Sp9712, but a precise estimate was only obtained for Sp9712. Using this feldspar Pb composition to correct the data results in dates scattering from ~ 20 to 54 Ma. However, particularly the dates above 23 Ma have a positive correlation to the fraction of non-radiogenic Pb, an indication that the chosen initial Pb isotopic composition may be not representative for the rutile. Applying this initial Pb correction, the resulting rutile dates are mostly Alpine with a suspected pre-Alpine component in the Alpe Sponda basement (see further discussion below). The U-Pb analyses do not form a well defined regression in an uncorrected Tera Wasserburg plots, and thus the composition of the initial Pb could not be calculated by this method. Pb-Pb isochrons also failed due to data scatter. Because of the low Pb radiogenic component in the rutile and the issue with initial Pb correction, the rutile U-Pb dates should be used and interpreted with extreme caution. Whenever possible, we prefer to rely on more robust age data from other mineral chronometers

7.2. Conditions of allanite, monazite and rutile formation

Constraining the condition of formation of allanite and monazite with respect to structures and metamorphism is crucial for age interpretation. During Alpine metamorphism, the peak temperatures were below 650°C in all investigated samples (Fig. 1), which is well below the closure temperature for the Th-U-Pb system in allanite (Gregory et al., 2012) and monazite (Rubatto et al., 2001). This is further confirmed for allanite by the presence of inherited ages in the Forcola orthogneisses and the Robiei gneiss Ba0901. Therefore, the obtained ages date the formation of the mineral growth zones. We use textural relationships and the trace element composition of monazite and allanite growth zones to constrain the reactions that took place during allanite-epidote growth and infer coexistence of accessory minerals and major phases such as garnet (e.g. Rubatto, 2002; Hermann and Rubatto, 2003; Buick et al., 2006). Zr-in-rutile thermometry can be used to relate rutile ages to metamorphic conditions. However, in the present case, age interpretation is complicated by the potential mixing of different rutile generations when 100s of grains are picked for isotope dilution analysis and the fact that Pb diffusion in rutile may occur at amphibolite-facies conditions over the relatively wide range of ~450 to 650 °C (e.g. Cherniak, 2000; Vry and Baker, 2006; Kooijman et al., 2010; Warren et al., 2012). Below we discuss the ages from across the area in chronological order, starting from Variscan metamorphic ages in the basement before discussing prograde Alpine allanite to higher temperature monazite.

Pre-Alpine monazite in Campolungo schists CLM-5 and 6 is aligned along the folded main foliation (Fig. 2e), which is partly wrapping the garnet, but is overgrown by staurolite and kyanite. In both samples monazite contains black micro inclusions of graphite, which occasionally defines a foliation that continues in the matrix (Fig 2c). This suggests that the Carboniferous monazite already formed as part of a metamorphic assemblage. The crystals are euhedral, flat prismatic in shape, with sharp edges and yield a single age and therefore a detrital origin is excluded. The ~330 Ma age in the two samples is interpreted as dating Variscan metamorphism in the Campolungo (Simano nappe) basement. It is surprising that no Alpine monazite has been found in both samples. Garnet in CLM-6 displays a core with concentric zoning that is separated from a nearly homogenous rim by an irregularly shaped annulus that is crosscutting the core. In the light of a pre-Alpine age of metamorphic monazite, this feature is interpreted as a phase of garnet resorption between the Variscan metamorphic event and the Alpine amphibolite facies metamorphism. Accordingly, the Variscan metamorphic conditions can be constrained to be of upper greenschist to lower amphibolite facies conditions based on the inclusion assemblage of chloritoid, chlorite and staurolite found in the garnet core. At these general conditions, rutile may have been the stable Ti phase. Formation of rutile during a Variscan event is suggested on the basis of the high apparent ages obtained in Alpe Sponda fels Sp9712, where two fractions containing darker rutile grains returned dates of ~ 52 to 57 Ma. Such spurious dates could be due to mixing between Alpine and Variscan rutile, possibly with partial Pb loss of the older population.

The pre-Alpine metamorphic event was overprinted during Alpine metamorphism by the amphibolite facies assemblage of muscovite-biotite-garnet-staurolite at only slightly higher metamorphic conditions. The main foliation S1 in schists CLM-5 and 6, that is parallel to the main foliation in the overlaying metamorphosed Mesozoic sediments, is therefore interpreted as a transposed pre-Alpine foliation. Gieré et al. (2011) reported very similar garnet and tourmaline textures with a Ca-rich annulus separating cores and rims from metapelites from the same area. As the protolith was assumed to be a Permo-Carbonferous sediment (and thus would have experienced only

Alpine metamorphism), they interpreted that the annulus was formed during Alpine prograde metamorphism at the transition from allanite to monazite. This is inconsistent with the new age data that shows that the rocks around Laghetto di Campolungo belong to the polymetamorphic basement of the Simano nappe and that no new monazite was formed by the Alpine metamorphic cycle. Indeed, the reported trace element compositions of monazite reported by Gieré et al. (2011) include 1200 ppm Pb, 42000 ppm Th and 5100 ppm U. The high amount of Pb is consistent with a Variscan age of the monazite rather than an Alpine age (that would result in at least an order of magnitude lower Pb content). Peak metamorphic temperatures for the Campolungo area have been constrained between 600 and 625°C based on multi-phase equilibria (Fig. 1; Todd and Engi 1997). On the other hand, Gieré et al. (2011) proposed a significantly higher peak T of 660°C concomitant with small amounts of partial melting. Partial melting is well known to enhance the recrystallization of monazite (Rubatto et al., 2001; Kelsey et al., 2008). The absence of leucosomes in the field and the lack of Alpine age monazite in these rocks are in better agreement with the lower peak metamorphic temperatures proposed by Todd and Engi (1997).

Early Alpine dates around 33-34 Ma were obtained from the two fractions of Alpe Sponda rutiles. In this sample, rutile is included both in large garnet grains (Grt I, II) and small garnet grains (Grt III). Zr-in-rutile thermometry returns ~ 550 °C for all Sp9712 rutile grains analysed (most likely including both > 50 Ma and 33-34 Ma rutile), which is significantly lower than the expected T_{max} for this area (~620 °C, Todd and Engi, 1997). This age has to be taken with caution, due to potential mixing with inherited components, but it is possible, and in line with allanite data, that 33-34 Ma rutile formed during a prograde stage at temperatures of ~ 550 °C.

The Alpine ages in the Campolungo area are constrained by accessory phases found in the metamorphosed Permo-Mesozoic sedimentary rocks. Allanite in the calcschist CLB-3 (31.7 ± 1.1 Ma) is included in Grt I and is aligned along the relic fabric preserved in garnet (S1, Fig. 2c); garnet grains are wrapped and rotated by the dominant foliation (S2). The allanite age is therefore interpreted to date prograde garnet growth as well as the relic foliation along which the allanite is aligned. The dominant foliation in this sample (S2) is correlated with the regional D2 (Grujic and Mancktelow, 1996; Maxelon and Mancktelow, 2005), the major deformation phase that refolded the nappe stack and is responsible for many of the major tectonic structures in the Lepontine dome. The relic foliation that is only preserved in garnet is likely to be S1, and the allanite age (31.7 ± 1.1 Ma) may reflect the timing of the regional D1 nappe stacking (Maxelon and Mancktelow, 2005). The HREE patterns in CLB-3 allanite cores are depleted (Fig. 5b), providing evidence that allanite cores grew during/after prograde garnet formation, which sequestered Mn and HREE.

Allanite in Campolungo quartzite Ma0901 (28.5 ± 1.3 Ma) is aligned along the dominant foliation of the rock, which is likely to be a composite S1/S2 fabric (S1 and S2 are approximately parallel; e.g. Maxelon and Mancktelow, 2005). Rutile is included in Ma0901 allanite cores and Zr-in-rutile thermometry indicates a temperature of ~ 575 °C, which is below the estimated temperature for T_{max} conditions (600-625°C, Todd and Engi, 1997). The allanite age is therefore interpreted to date a stage in the prograde history of the rock during major tectonic reworking of the nappe pile (D2, Grujic and Mancktelow, 1996; Maxelon and Mancktelow, 2005). Although garnet is not abundant in the sample, the HREE depletion of allanite provides evidence that garnet was present at the time of allanite formation (Fig. 5c).

The presence of relic igneous allanite in the Forcola orthogneisses and the Robiei gneiss Ba0901 (the bulk composition of which is similar to orthogneiss, Table A1) indicates that, in these samples, igneous allanite is the precursor to metamorphic allanite. In the Robiei gneiss (Ba0901), metamorphic allanite cores (26.8 ± 1.3 Ma) formed during prograde metamorphism and contain inclusions of biotite and muscovite. Allanite domains in this sample show only a small decrease in total REE concentration from cores through mantles and rims. It is speculated that allanite rims (19.7 ± 1.3 Ma) formed by resorption whereby the allanite was partially consumed and recrystallised as LREE allanite rims near T_{max} conditions. This resorption likely occurred with very little volume change (i.e. REE in allanite were neither concentrated nor diluted during resorption). In this sample K-feldspar and plagioclase are fresh, indicating minimal fluid influx during retrogression.

Rutile from Robiei calcschist (Ba0903A; Bündnerschiefer) returns TIMS dates that span from 27 to 21 Ma – almost the entire range of allanite and monazite ages in the western samples. Zr-in-rutile thermometry indicates that rutile crystallised over a limited temperature range from 565 to 595 °C. The Zr-in-rutile temperatures overlap with the expected T_{max} for this area, based on multiphase equilibria thermobarometry (Figure 1; Todd and Engi, 1997). Galli et al. (2007) investigated in detail the structures and metamorphism of Bündnerschiefer in the Naret region, which is situated 5 km to the northeast of Robiei. They proposed that main recrystallization of minerals (including rutile) occurred between D2 and D3 and T_{max} of 650 °C. The range of rutile dates is consistent with either several episodes of rutile recrystallization during the D1-D3 deformation events or partial Pb loss from an early (>27 Ma) rutile generation formed during prograde metamorphism.

Forcola orthogneiss allanite (scattering dates 25-32 Ma) is aligned along S1, a dominant and early foliation. However, the timing of allanite crystallisation with respect to metamorphic phase and deformation history is complicated by the large variety of internal textures of allanite (Fig. 3f-h). The mosaic allanite from LEP0980 has a unique texture of subgrain cores and rims, which reflect two allanite growth stages that occurred at 31.3 ± 1.1 Ma for the cores and younger in the rims. Analyses from the regularly zoned allanite from the same sample do not define an isochron age and single spot dates span the entire range of mosaic allanite ages (25-32 Ma). There is no correlation between the age of regularly zoned allanite and internal texture (i.e. core vs. rim). It is possible that the older dates are the result of Pb inherited from a precursor phase (Romer and Siegesmund, 2003), and thus these ages are not further considered in the discussion. In allanite from sample LEP0807 there is no correlation between Th-Pb age and internal texture (core vs. rim) and all analyses defined a Th-isochron age of 27.4 ± 0.6 Ma suggesting that any difference in age between allanite core and rim is below the resolution of the analyses.

Croveo schist (Ma9330) monazite age of 21.7 ± 0.3 Ma is interpreted to date the timing of monazite crystallisation at the expense of allanite. Allanite as a precursor to monazite (see also Romer and Siegesmund, 2003; Janots et al., 2008) is inferred from the presence of relic allanite included in garnet. The HREE pattern of monazite is depleted with respect to the bulk rock, suggesting that garnet was still stable when monazite was forming (Fig. 5h). Additionally, the negative Eu anomaly is more pronounced in monazite than in the bulk rock and thus plagioclase was also stable. As garnet and plagioclase are peak metamorphic minerals, it is reasonable to assume that monazite formed close to T_{max} conditions of 620°C at 6.2 kbar (Todd and Engi, 1997).

The paragneisses of Alpe Sponda belong to the basement of the Simano nappe and thus it is plausible that these samples underwent polymetamorphism as is the case for the Campolungo metapelites (see above). Element maps as well as trace element profiles through the large garnet grains suggest that Grt I has been resorbed prior to the formation of Grt II rims and newly formed Grt III. This is very similar to the two generations of garnet found in sample CLM-6, where a pre-Alpine garnet core is truncated by an Alpine rim. Two distinct types of garnets with the same compositional characteristics as in our study (Fig. 4g-h) have been reported by Beitter et al. (2008) from the Alpe Sponda area. Beitter et al. (2008) report garnet grains corresponding to Grt I were only found in the paragneiss whereas grains corresponding to Grt III were associated to the Alpine rutile-kyanite-quartz veins.

Allanite is a precursor to monazite in Alpe Sponda fels Sp9712. Rare allanite has been observed in the garnet whereas no monazite is observed as inclusions in garnet. The assembly of small monazite grains that satellite relic allanite (Fig. 3e) also indicates that monazite replaced allanite in these rocks. The Alpe Sponda fels monazite (22.0 ± 0.3 Ma) returned the youngest ages of the Central samples. The steady increase of Dy/Lu and an associated increase of the negative Eu anomaly (Fig. 5h) suggest that these monazites formed together with garnet and plagioclase, the peak assemblage. Thus, we conclude that peak metamorphic conditions persisted up to 22 Ma in this area.

Campolungo calcschist (CLB-4) returned rutile dates between 19-25 Ma. Rutile crystallised after garnet (one of the earliest prograde minerals preserved) and before staurolite (one of the later-stage minerals). The Zr-in-rutile temperature for CLB-4 is ~ 625 °C, similar to the estimate for maximum Barrovian temperature conditions in this area (600-620 °C; Todd and Engi, 1997). The spread of rutile dates may again reflect protracted rutile crystallisation during slow heating while temperatures approached T_{max} and/or cooling ages.

7.3. Implications for the allanite-to-monazite transition in metamorphic rocks

Our regional scale data set provides an excellent framework to shed light on the nature of the allanite-to-monazite transition during Barrovian metamorphism (Fig. 9). Rutile inclusions in allanite from Campolungo Ma0901 quartzite provide evidence that the crystallisation of allanite cores occurred at a temperature of ~ 575 °C, as determined by Zr-in-rutile thermometry of rutile inclusions. Moreover, the similarity of the allanite ages from the calcschist and quartzite (~ 32 Ma and ~ 28 Ma respectively) and their textural positions associated with the amphibolite facies S1 and S2 foliation, indicates that allanite crystallisation in the calcschist did not occur at the low temperatures of 400-450 °C suggested by previous studies of prograde allanite (e.g. Smith and Berreiro, 1990; Wing et al., 2003; Janots et al., 2008; Rasmussen and Muhling, 2009; Janots et al., 2011).

Robiei gneiss (Ba0901) allanite is an example of two separate phases of allanite crystallisation in the same rock under different conditions. Allanite prevails in this rock, which contains very little Ca (0.74 %), and has a low Ca/Al ratio of 0.08. At the metamorphic conditions attained and for a rock of this bulk composition, the models of both Spear (2010) and Wing et al. (2003) predict monazite stability (Fig. 9). It is inferred that allanite rims crystallised (instead of monazite) at the expense of allanite because T_{max} was too low for monazite stability in this sample (T_{max} ~ 575 °C).

Monazite crystallisation in samples Ma9330 and Sp9712 is interpreted to have occurred close to T_{max} conditions (~ 620 °C). This is somewhat higher than the reaction temperatures suggested by previous studies of natural samples (560-580 °C in Janots et al., 2008; ~ 540 °C in Gieré et al., 2011) and in thermodynamic models (Spear 2010). The model of Spear (2010) proposes a temperature range of 400 to 700 °C for the allanite-to-monazite reaction, depending on bulk Ca, Al and pressure (Fig. 9a,b). For bulk composition of sample Ma9330 (Table A1) the model predicts that the allanite-to-monazite reaction would occur at ~ 450 °C (P = 5 kbar); at 10 kbar the reaction is predicted to occur at ~ 500 °C. However the model assumes simple systems and the studied samples are more complex; neither of the reaction temperature predictions is consistent with our observations. Furthermore, the model predicts that the reaction would have occurred even in samples where allanite is the stable REE mineral (Fig. 9a,b). Spear and Pyle (2010) admit that good thermodynamic data for allanite is lacking and the disagreement between observations in this study and predicted reaction temperatures may be due to the thermodynamic data used. One of the major limitations in applying thermodynamic models to accessory mineral reactions is the difficulty in defining the reactive bulk composition. Particularly for minerals whose stabilities are controlled by trace elements, their reactive bulk is likely not equivalent to the rock composition and local difference in trace element distributions will have major consequences on accessory mineral reactions. Additionally, deformation and partial hydration may localize reactions. The survival of Carboniferous monazite in Campolungo samples CLM-5 and 6 provides evidence that in these basement samples no Alpine prograde allanite formed. This might be related to a limited retrogression/hydration of these amphibolite facies schists postdating the Variscan orogeny. In contrast, Alpe Sponda sample Sp9712 contains exclusively Alpine monazite that has relic allanite included, indicating an Alpine prograde growth of monazite from allanite.

It has been proposed that bulk composition (especially Ca concentration and Ca/Al ratio) plays a key role for the allanite to monazite transition (Wing et al., 2003). This effect may explain allanite stabilisation at lower T in the calcschist than in the quartzite, but this model only holds for the Campolungo samples. CaO contents and Ca/Al ratio do not account for allanite's perpetuation or its replacement by monazite in all samples. The monazite- and allanite- stable areas in Ca/Al space proposed by Wing et al. (2003) do not hold for Central Alps samples studied here (Fig. 9c) and by Janots et al. (2008, 2011). This is a strong indication that the reactive bulk composition may play a significant role in accessory mineral stability.

The inconsistencies between conclusions reached from the study of natural samples and those from thermodynamic models show that not enough is known about the factors governing allanite and monazite stability to predict the conditions of allanite-in and monazite-in reactions in pelitic to granitic compositions. This reinforces the need for sample-specific petrological considerations (e.g. textural relationships, deformation, effective reactive bulk) in order to link accessory mineral ages with metamorphism.

7.4. Trend of ages across the Lepontine dome

A regional pattern for Barrovian metamorphism develops when the histories of the Croveo-Robiei and Campolungo-Sponda samples are combined with studies from the literature (Fig. 10). Excluding ages from the Southern Steep Belt (SSB), crystallisation ages fall into two groups: older ages (27 to 33 Ma) are interpreted as prograde ages that relate to major, orogen-scale tectonic movements (nappe stacking) and younger ages that can be linked to post-collisional mineral growth close to T_{max}. Prograde allanite ages are in good agreement with the 29-32 Ma Th-Pb allanite ages of Janots et al. (2009) and a greenschist facies K-Ar amphibole age of 29 ± 3 Ma (Deutsch and Steiger, 1985), both from the Northern Steep Belt (NSB).

U-Pb garnet ages of Vance and O'Nions (1992) from the NSB also agree with prograde allanite ages from this study. The garnet investigated by Vance and O'Nions (1992) are re-interpreted as prograde based on the petrological relationships described in that study (i.e. garnet is pre- to synkinematic with the dominant foliation), which are similar to petrological relationships of samples from the current study, in which garnet is a prograde phase.

These prograde ages in the northern part of the Lepontine belt coincide with the age of post-HP greenschist-facies overprint dated in Valaisan units in the northeastern Lepontine (Wiederkehr et al., 2009). In the north, progressive regional metamorphism thus reached greenschist-facies conditions within 2-10 Ma after HP metamorphism in the Valaisan units (Wiederkehr et al., 2009), and in Cima Lunga and Adula melange units (Fig. 10, Becker, 1993; Gebauer, 1996; Brouwer et al., 2005; Hermann et al., 2006; Liati et al., 2009). However, the Valaisan units showing HP metamorphism, as well as the mélange units, were exhumed prior to their Barrovian overprint , which postdates nappe emplacement. The correlation of allanite ages with dominant deformation structures suggests that the main deformation event occurred during this time interval, i.e. 32-27 Ma ("stage 2" of Berger et al., 2011); isoclinal refolding of the nappes probably initiated during the later part of this phase. The resolution of ages is not sufficient to evaluate whether there is an E-W age progression in the nappe stacking phase, but a S-N younging of the main deformational phases has been previously established (Berger et al., 2011).

The thermal peak followed nappe stacking and maximum ages for this stage are recorded by monazite and a minimum age by Ba0901 allanite rims (Fig. 10). Isograds are clearly discordant to the structures established during the nappe stacking events, providing evidence on a regional scale that thermal metamorphism outlasted this deformation event (Fig. 11a). The regional scale, south-west verging, ductile transverse folding (F4 of Steck et al., 2013) likely occurred close to T_{max}. Combining formation ages that likely record a stage close to maximum T from this study with well-constrained ages from the literature, especially additional monazite ages from further south (Köppel and Grünenfelder, 1975) reveals a consistent trend with metamorphic grade (Fig. 11b). As outlined by the dashed line, younger ages (18-20 Ma) are found in the lower grade rocks (T_{max} = 550-580°C) of the north, and older ages (21-23 Ma) occur in the higher grade rocks (T_{max} = 590-650°C) towards the middle and southern part of the Barrovian sequence.

The general trend for crystallisation ages does not apply to rocks of the SSB. Ages for the SSB migmatisation span the entire age range of prograde and T_{max} ages from the subsolidus rocks (Figs. 11 and 12). The spread of ages from 22 to 32 Ma for migmatites has been interpreted to reflect an extended period of upper-amphibolite facies metamorphism with protracted incipient melting during various deformation stages in the SSB (Rubatto et al., 2009; Gregory et al., 2012). Partial melting persisted to 22 Ma, indicating that the rocks resided above the wet solidus (T ≥ 650°C). It should be noted that fission track data (Hurford 1986) show ages around 19 Ma for the partial annealing of zircon in samples from the SSB, reflecting cooling rates >100 °C/Ma for that part of the Lepontine dome.

The emerging picture for the age of Barrovian metamorphism for the Lepontine dome is that high temperatures in the southern and central areas lasted to 21-23 Ma, whereas in the north-western part they are slightly younger with ages of 18-20 Ma. The combined age data for main deformations and T_{max} thus suggest that, at least in the central and southern Lepontine, amphibolite-facies conditions were retained for up to 10 Ma after nappe stacking, allowing for multiple phases of ductile deformation (Steck et al., 2013). At ~20 Ma, late-orogenic shortening and uplift was accommodated by intense phases of folding, associated with backthrusting in the south, thus producing the two steep belts (SSB and NSB; Berger et al., 2011).

Ages of Hurford (1986) and Steck and Hunziker (1994) suggest that rocks of the Croveo-Robiei area had cooled below retention of Rb-Sr in biotite (~ 300 °C) by ~15 Ma and below ~250 °C by ~ 12-15 Ma (zircon fission track). Hurford (1986) also reports a Rb/Sr muscovite age of ~ 18 Ma (T ≈ 500 °C, Hurford, 1986) for samples to the East of Ma9330 (Fig. 10b). Similarly, rapid cooling to below ~ 250 °C by 10-13 Ma is documented for the Campolungo-Sponda area (Hurford, 1986; Janots et al., 2009; Fig. 10). Therefore, the Central and Northern part of the Lepontine dome must have experienced very rapid cooling after ~20 Ma.

Insight into the cooling history of the eastern samples is provided by Ar-Ar white mica ages from the same samples, as well as one sample from the hanging wall of the Forcola fault (which contain no Alpine allanite). White mica from the hanging wall and footwall of the Forcola fault return Ar-Ar ages of 27-25 Ma and 22-21 Ma respectively (Augenstein, 2013). The younger age in the footwall is interpreted to reflect the onset of grain size reduction and mylonitisation along the Forcola fault (Augenstein, 2013). The Ar-Ar ages also suggest that temperatures were below Ar retention in white mica at 22-

21 Ma for the Forcola rocks. K-Ar ages of biotite in this area are around 20 Ma (Steck and Hunziker, 1994) and provide further evidence for rapid cooling. In an east-west traverse, the K-Ar ages of biotite are progressively younger towards the west, suggesting that cooling propagated from east to west (Steck et al., 2013).

The accelerated cooling at about 20 Ma, observed throughout the Lepontine dome, did not result in an increased sedimentation rate as would be expected if cooling was a result of increased uplift, erosion and associated exhumation. In contrast, the detailed study of the stratigraphy in the foreland basins surrounding the Lepontine dome reveals that erosion rates decreased by about 50 % at 20 Ma (Schlunegger, 1999). Therefore, the fast cooling around 20 Ma is likely related to exhumation of the Central Alps during a phase of transtensional tectonics (Ciancaleoni and Marquer, 2008). This exhumation might have been accommodated by nearly simultaneous top-to-the-West normal faulting along the Simplon normal fault (Mancktelow, 1992), vertical displacement during back thrusting along the Insubric Line (Schmid et al., 1989) and perhaps normal fault movement on the Forcola line (Ciancaleoni and Marquer, 2008). In any case, the tight age constraints for the transition from low-grade metamorphism to amphibolite-facies conditions across the Central Alps (Figs. 11, 12) provide powerful constraints for the interpretation of this classical orogeny.

Acknowledgements

The authors acknowledge the technical assistance of Robert Rapp for EMP analysis, Charlotte Allens for LA-ICP-MS analysis and Peter Holden for SHRIMP analysis. Fernando Corfu is thanked for comments on a previous version of the manuscript. Constructive comments from Antonio Langone and an anonymous reviewer and editorial handling by M. Scambelluri are acknowledged.

Table captions

Table 1: Sample overview showing the main and accessory mineral assemblage, the minerals used for dating and the results of U-Th-Pb geochronology.

Figure captions

Figure 1: (a) Tectonic overview of the Central Alps and sample locations (after Trommsdorf et al., 2000; Berger et al., 2005; Burri et al., 2005; Maxelon and Mancktelow, 2005; Janots et al., 2008). (b) Central Alps map with isotherms for Barrovian metamorphism that overprinted the major tectonic boundaries (Todd and Engi, 1997) and sample numbers. Swiss grid coordinates are in kilometres. For a colour version of the Figure please refer to the online version of the article.

Figure 2: Photomicrographs of (a) Ma9330 S2 white micas and biotite wrapping garnet (note that S1 and S2 are sub-parallel in these samples); (b) CLB-3 garnet, which preserves internal S1 fabric, rotated and wrapped by S2 white mica and biotite; (c) Monazite crystal in CLM-6 that is aligned along the main foliation defined by micas and graphite; (d) Ma0901 allanite aligned along the S1/S2 fabric; (e) Sp9712 large staurolite crystals surrounding kyanite that is partially replaced by white mica; (f) LEP0980 allanite aligned along the dominant fabric (S1). A detailed petrographic description of the samples is given in the electronic Appendix.

Figure 3: (a) Backscatter electron (BSE) image and (b) compositional map of Ba0901 allanite showing an allanite rich-core (C), epidote mantle (M) and allanite rim (R). BSE images of (c) CLB-3 allanite; (d) Ma0901 allanite, arrows point to rutile inclusions in the allanite core; (e) Sp9712 monazite satellites of a relic allanite; (f)

LEP0979 allanite rims on epidote-rich cores; (g) LEP0807 allanite; (h) LEP0980 mosaic allanite and regularly zoned allanite (P = pre-Alpine relics).

Figure 4: Garnet composition (data from Table A2). Ma9330 garnet: (a) MgO, MnO and Lu profile across the garnet; O. Rim = outer rim of the garnet; (b) chondrite-normalised REE, the systematic depletion in HREE from core (C) to rim (R) is indicated by the arrow; outer rim garnet is mildly enriched in MREE. (c) MgO, MnO and Lu profile across CLB-3 garnet, showing a sharp increase in Lu from Grt I rim to Grt II; (d) chondrite-normalised REE patterns of CLB-3 garnet. (e) MgO, MnO and CaO profile across CLM-6 garnet. The co-rim boundaries (vertical dashed lines) are based on the element map shown in (f). (f) element distribution map of Ca in garnet from CLM-6. Note the Alpine rim cutting across the regular zoning in the pre-Alpine core. (g) LA ICPMS profile across Sp9712 Grt I and II; location of the profile is given in the Ca map (inset). I_C, I_R = Grt I core and rim respectively, II_C = Grt II core etc. (f) Sp9712 chondrite-normalised REE patterns of garnets I-III. Inset shows Ca map of Grt III. The decrease in HREE from core to rim is indicated.

Figure 5: Chondrite-normalised REE composition of accessory allanite (a-f) and monazite (g-h) compared with whole rock (WR). REE of allanite cores, mantles and rims of (a) Ba0901, (b) CLB-3 and (c) Ma0901. (d) A comparison of allanite growth zones in terms of REE and Th/U in metasediments. REE of allanite in Forcola orthogneiss samples (e) LEP0807 and LEP0979 and (f) LEP0980. (g) REE of monazite in Croveo schist (Ma9330) and Alpe Sponda fels (Sp9712). (h) REE compositional variation in Alpine monazite. The effect of feldspar and garnet coexistence is indicated with arrows.

Figure 6: Summary of geochronology results grouped by area (Western, Central and Eastern Lepontine) and by phase dated. Monazite and allanite ages are formation ages, whereas rutile dates are more difficult to interpret, see text for discussion.

Figure 7: Monazite ages. (a) Concordia plot for monazite analyses in samples CLM-5 and CLM-6 (a), in sample Ma9330 (b) and in sample Sp9712. Average $^{206}Pb/^{238}U$ ages are given in (a), concordia ages are given in (b) and (c) and are represented by the blue ellipses. The unfilled ellipses in (a) and (c) are not used for age calculation. A representative BSE image of dated monazite is shown on the right of plot (a) and (c).

Figure 8: Allanite Th-Pb isochrons for (a) Ba0901 allanite cores; (b) Ba0901 allanite rims; (c) CLB-3 allanite cores; (d) Ma0901 allanite cores; (e) LEP0980 mosaic allanite cores; (f) LEP0807 allanite (cores and rims). The model common Pb composition (Stacey and Kramers, 1975) is indicated on the y-axis and always close to the intercept defined by the isochron. Error ellipses are 2σ; errors quoted on isochron ages are 95 % confidence.

Figure 9: Allanite- and monazite-bearing samples of Alpine age compared to modelled stability fields. (a) Samples plotted in terms of temperature and bulk-rock CaO with stability fields calculated by Spear (2010). Numbers next to symbols are wt % Al_2O_3. Reaction lines of Spear (2010) were calculated for 5 kbar pressure; the reaction is predicted to occur at higher temperature with increasing bulk CaO, and the slope is dependent on bulk Al_2O_3. (b) Samples plotted in the allanite-monazite P-T stability field of Spear (2010). Numbers indicate the sample whole rock CaO concentration (wt %); more than one number next to a symbol indicates more than one sample from the same locality. Two reaction curves are plotted: one for low CaO and one for moderate Ca concentration. (c) Al/Al_{Shaw} vs. Ca/Ca_{Shaw}, where Al_{Shaw} and Ca_{Shaw} are concentrations for

an "average pelite" (Shaw, 1956). The discrimination line of Wing et al. (2003) shows the expected stability of allanite and monazite for rocks in andesite, kyanite and sillimanite zones. None of the diagrams predicts correctly the allanite or monazite presence in the studied samples.

Figure 10: Summary of Alpine metamorphism in the Central Alps. (a) An overview of interpretation of metamorphic ages in the Lepontine Alps; (b) Temperature-time paths for samples studied as well as for the Southern Steep Belt (SSB), Northern Steep Belt (NSB) and the Urseren zone, taken from the literature as indicated. (1) Becker, 1993; (2) Gebauer, 1996; (3) Brouwer et al., 2005; (4) Wiederkehr et al., 2009; (5) Deutsch and Steiger, 1985; (6) Janots et al., 2009; (7) Vance and O'Nions, 1992; (8) Janots and Rubatto, 2014; (9) Köppel and Grünenfelder, 1975; (10) Hurford, 1986; (11) Liati et al., 2000; (12) von Blanckenburg, 1992; (13) Oberli et al., 2004; (14) Gregory et al., 2012; (15) Rubatto et al., 2009; (16) Augenstein, 2013.

Figure 11: Trend of ages across the Lepontine dome. (a) Map of isotherms with locations of samples included in (b). Note that the study site of Janots and Rubatto (2014) is north of the map area. (b) Metamorphic grade (T_{max}) vs. allanite, monazite and zircon crystallisation age from this and selected studies from the literature as indicated. Legend is the same for both (a) and (b).

TO BE PRINTED IN COLOUR

Figure 1

Figure 2

Figure 3

Figure 10

Figure 11

References

Allaz, J., Engi, M., Berger, A., Villa, I.M., 2011. The effects of retrograde reactions and of diffusion on ^{40}Ar-^{39}Ar ages of micas. Journal of Petrology, 52, 691-716.

Augenstein, C., 2013. The formation of the Lepontine gneiss dome. Ph.D. dissertation, Australian National University, Canberra, Australia.

Becker, H., 1993. Garnet peridotite and eclogite Sm-Nd mineral ages from the Lepontine dome (Swiss Alps): New evidence for Eocene high-pressure metamorphism in the central Alps. Geology, 21, 599-602.

Beitter, T., Wagner, T., Markl, G., 2008. Formation of kyanite-quartz veins of the Alpe Sponda, Central Alps, Switzerland: implications for Al transport during regional metamorphism. Contributions to Mineralogy and Petrology, 156, 689-707.

Berger, A., Mercolli, I., Engi, M., 2005. The central Lepontine Alps: Notes accompanying the tectonic and petrographic map sheet Sopra Ceneri (1:100'000). Schweizerische Mineralogische und Petrographische Mitteilungen, 85, 109-146.

Berger, A., Schmid, S.M., Engi, M., Bousquet, R., Wiederkehr, M., 2011. Mechanisms of mass and heat transport during Barrovian metamorphism: A discussion based on field evidence from the Central Alps (Switzerland/northern Italy). Tectonics, 30, TC1007.

Brouwer, F.M., Burri, T., Engi, M., Berger, A., 2005. Eclogite relics in the Central Alps: PT - evolution, Lu–Hf ages and implications for formation of tectonic mélange zones. Schweizerische Mineralogische und Petrographische Mitteilungen, 85, 147-174.

Brouwer, F.M., van de Zedde, D.M.A., Wortel, M.J.R., Vissers, R.L.M., 2004. Late-orogenic heating during exhumation: Alpine PTt trajectories and thermomechanical models. Earth and Planetary Science Letters, 220, 185-199.

Budzyn, B., Hetherington, C.J., Williams, M.L., Jercinovic, M.J., Michalik, M., 2010. Fluid-mineral interactions and constraints on monazite alteration during metamorphism. Mineralogical Magazine, 74, 659-681.

Buick, I.S., Hermann, J., Williams, I.S., Gibson, R., Rubatto, D., 2006. A SHRIMP U–Pb and LA-ICP-MS trace element study of the petrogenesis of garnet–cordierite–orthoamphibole gneisses from the Central Zone of the Limpopo Belt, South Africa. Lithos, 88, 150-172.

Burri, T., Berger, A., Engi, M., 2005. Tertiary migmatites in the Central Alps: Regional distribution, field relations, conditions of formation, and tectonic implications. Schweizerische Mineralogische und Petrographische Mitteilungen, 85, 215-232.

Ciancaleoni, L.,Marquer, D., 2008. Late Oligocene to early Miocene lateral extrusion at the eastern border of the Lepontine Dome of the Central Alps (Bergell and Insubric areas, eastern Central Alps). Tectonics, 27, TC4008.

Cherniak, D.J., 2000. Pb diffusion in rutile. Contributions to Mineralogy and Petrology 139, 198-207.

Deutsch, A., Steiger, R.H., 1985. Hornblende K-Ar ages and the climax of Tertiary metamorphism in the Lepontine Alps (south-central Switzerland) an old problem reassessed. Earth and Planetary Science Letters, 72, 175-189.

Engi, M., 2017. Petrochronology based on REE-minerals: Monazite, allanite, xenotime, apatite. Reviews in Mineralogy and Geochemistry 83, in press.

Engi, M., Todd, C.S., Schmatz, D., 1995. Tertiary metamorphic conditions in the eastern Lepontine Alps. Schweizerische Mineralogische und Petrographische Mitteilungen, 75, 347-396.

Ewing T.A., Hermann, J., Rubatto, D., 2013. The robustness of the Zr-in-rutile and Ti-in-zircon thermometers during high-temperature metamorphism (Ivrea-Verbano Zone, northern Italy). Contributions to Mineralogy and Petrology, 165, 757-779.

Ferry, J.M., Watson, E.B., 2007. New thermodynamic models and revised calibrations for the Ti-in-zircon and Zr-in-rutile thermometers. Contributions to Mineralogy and Petrology, 154, 429-437.

Finger, F., Broska, I., Roberts, M.P., Schermaier, A., 1998. Replacement of primary monazite by apatite-allanite-epidote coronas in an amphibolite facies granite gneiss from the eastern Alps. American Mineralogist, 83, 248-258.

Foster, G., Gibson, H.D., Parrish, R., Horstwood, M., Fraser, J., Tindle, A., 2002. Textural, chemical and isotopic insights into the nature and behaviour of metamorphic monazite. Chemical Geology, 191, 183-207.

Frey, M., Bucher, K., Frank, E., Mullis, J., 1980. Alpine metamorphism along the Geotraverse Basel-Chiasso – a review. Eclogae Geologicae Helvetiae, 73, 527-546.

Frey, M., Hunziker, J.C., Frank, W., Bocquet, J., Dal Piaz, G.V., Jäger, E., Niggli, E., 1974. Alpine metamorphism in the Alps: A review. Schweizerische Mineralogische und Petrographische Mitteilungen, 54, 247-290.

Galli, A., Mancktelow, N., Reusser, E., Caddick, M., 2007. Structural geology and petrography of the Naret region (northern Valle Maggia, N.Ticino, Switzerland). Swiss Journal of Geosciences, 100, 53-70.

Garofalo, P.S., 2012. The composition of Alpine marine sediments (Bündnerschiefer Formation, W Alps) and the mobility of their chemical components during orogenic metamorphism. Lithos, 128-131, 55-72.

Gebauer, D., 1996. A P-T-t Path for an (ultra?-) high-pressure ultramafic/mafic rock-association and its felsic country-rocks based on SHRIMP-dating of magmatic and metamorphic zircon domains. Example: Alpe Arami (Central Swizz Alps). In A. Basu, and S. Hart (Eds.), Earth processes: Reading the isotopic code, American Geophysical Union Monograph 95, pp. 307-329.

Gieré, R., Rumble, D., Günther, D., Connolly, J., Caddick, M.J., 2011. Correlation of growth and breakdown of major and accessory minerals in metapelites from Campolungo, Central Alps. Journal of Petrology, 52, 2293-2334.

Gregory, C.J., Rubatto, D., Allen, C.M., Williams, I.S., Hermann, J., Ireland, T., 2007. Allanite micro-geochronology: A LA-ICP-MS and SHRIMP U-Th-Pb study. Chemical Geology, 245, 162-182.

Gregory, C.J., Rubatto, D., Hermann, J., Berger, A., Engi, M., 2012. Allanite behaviour during incipient melting in the southern Central Alps. Geochimica et Cosmochimica Acta, 84, 433-458.

Grujic, D., Mancktelow, N.S., 1996. Structure of the northern Maggia and Lebendun Nappes, Central Alps, Switzerland. Eclogae Geologicae Helvetiae, 89, 461-504.

Hermann, J., Rubatto, D., 2003. Relating zircon and monazite domains to garnet growth zones: age and duration of granulite facies metamorphism in the Val Malenco lower crust. Journal of metamorphic Geology, 21, 833-852.

Hermann, J., Rubatto, D., Trommsdorff, V., 2006. Sub-solidus Oligocene zircon formation in garnet peridotite during fast decompression and fluid infiltration (Duria, Central Alps). Mineralogy and Petrology, 88, 181-206.

Hunziker, J.C., 1969. Rb/Sr Altersbestimmungen aus den Walliser Alpen. Hellglimmer- und Gesamtgesteinsalterswerte. Eclogae Geologicae Helvetiae, 62, 527-542.

Hurford, A.J., 1986. Cooling and uplift patterns in the Lepontine Alps South Central Switzerland and an age of vertical movement on the Insubric fault line. Contributions to Mineralogy and Petrology, 92, 413-427.

Jäger, E., 1973. Die alpine Orogenese im Lichte der radiometrischen Altersbestimmung. Eclogae Geologicae Helvetiae, 66, 11-21.

Janots, E., Berger, A., Engi, M., 2011. Physico-chemical control on the REE minerals in chloritoid-grade metasediments from a single outcrop (Central Alps, Switzerland). Lithos, 121, 1-11.

Janots, E., Brunet, F., Goffé, B., Poinssot, C., Burchard, M., Cemič, L., 2007. Thermochemistry of monazite-(La) and dissakisite-(La): implications for monazite and allanite stability in metapelites. Contributions to Mineralogy and Petrology, 154, 1-14.

Janots, E., Engi, M., Berger, A., Allaz, J., Schwartz, J.-O., Spandler, C., 2008. Prograde metamorphic sequence of REE minerals in pelitic rocks of the Central Alps: implications for allanite–monazite–xenotime phase relations from 250 to 610 °C. Journal of metamorphic Geology, 26, 509-526.

Janots, E., Engi, M., Rubatto, D., Berger, A., Gregory, C., Rahn, M., 2009. Metamorphic rates in collisional orogeny from in situ allanite and monazite dating. Geology, 37, 11-14.

Janots, E., Rubatto, D., 2014. U–Th–Pb dating of collision in the external Alpine domains (Urseren zone, Switzerland) using low temperature allanite and monazite. Lithos, 184-187, 155-166.

Kelsey, D.E., Clark, C., Hand, M., 2008. Thermobarometric modelling of zircon and monazite growth in melt-bearing systems: examples using model metapelitic and metapsammitic granulites. Journal of Metamorphic Geology, 26, 199-212.

Kim, Y., Yi, K., Cho, M., 2009. Parageneses and Th-U distributions among allanite, monazite, and xenotime in Barrovian-type metapelites, Imjingang belt, central Korea. American Mineralogist, 94, 430-438.

Kooijman, E., Mezger, K., Berndt, J., 2010. Constraints on the U-Pb systematics of metamorphic rutile from in situ LA-ICP-MS analysis. Earth and Planetary Science Letters, 293, 321-330.

Köppel, V., Grünenfelder, M., 1975. Concordant U-Pb ages of monazite and xenotime from the Central Alps and the timing of high temperature Alpine metamorphism, a preliminary report. Schweizerische Mineralogische und Petrographische Mitteilungen, 55, 129-132.

Liati, A., Gebauer, D., Fanning, C.M., 2000. U-Pb SHRIMP dating of zircon from the Novate granite (Bergell, Central Alps): evidence for Oligocene-Miocene magmatism, Jurassic/Cretaceous continental rifting and opening of the Valais trough. Schweizerische Mineralogische und Petrographische Mitteilungen, 80, 305-316.

Liati, A., Gebauer, D., Fanning, C.M., 2009. Geochronological evolution of HP metamorphic rocks of the Adula nappe, Central Alps, in pre-Alpine and Alpine subduction cycles. Journal of the Geological Society, London, 166, 797-810.

Mancktelow, N.S., 1992. Neogene lateral extension during convergence in the Central Alps: Evidence from interrelated faulting and backfolding around the Simplonpass (Switzerland). Tectonophysics, 215, 295-317.

Maxelon, M., Mancktelow, N.S., 2005. Three-dimensional geometry and tectonostratigraphy of the Pennine zone, Central Alps, Switzerland and Northern Italy. Earth Science Reviews, 71, 171-227.

Nagel, T., de Capitani, C., Frey, M., 2002. Isograd and P-T evolution in the eastern Lepontine Alps (Graubünden, Switzerland). Journal of metamorphic Geology, 20, 309-324.

Niggli, E., Niggli, C.R., 1965. Karten der Verbreitung einiger Mineralien der alpidischen Metamorphose in den Schweizer Alpen (Stilpnomelan, Alkali-Amphibol, Chloritoid, Staurolith, Disthen, Sillimanit). Eclogae Geologicae Helvetiae, 58, 335-368.

Oberli, F., Meier, M., Berger, A., Rosenberg, C., Gieré, R., 2004. U-Th-Pb and $^{230}Th/^{238}U$ disequilibrium isotope systematics: Precise accessory mineral chronology and melt evolution tracing in the Alpine Bergell intrusion. Geochimica et Cosmochimica Acta, 68, 2543-2560.

Pollington, A.D., Baxter, E.F., 2010. High resolution Sm–Nd garnet geochronology reveals the uneven pace of tectonometamorphic processes. Earth and Planetary Science Letters, 293, 63-71.

Rasmussen, B., Muhling, J.R., 2009. Reactions destroying detrital monazite in greenschist-facies sandstones from the Witwatersrand basin, South Africa. Chemical Geology, 264, 311-327.

Regis, D., Rubatto, D., Darling, J., Cenki-Tok, B., Zucali, M., Engi, M., 2014. Multiple metamorphic stages within an eclogite-facies terrane (Sesia Zone, Western Alps) revealed by Th-U-Pb petrochronology. Journal of Petrology, 55, 1429-1456.

Romer, R. L., Rötzler, J., 2011. The role of element distribution for the isotopic dating of metamorphic minerals. European Journal of Mineralogy, 23, 17-33.

Romer, R.L., Schärer, U., Steck, A., 1996. Alpine and pre-Alpine magmatism in the root-zone of the western Central Alps. Contributions to Mineralogy and Petrology, 123, 138-158.

Romer, R.L., Siegesmund, S., 2003. Why allanite may swindle about its true age. Contributions to Mineralogy and Petrology, 146, 297-307.

Rubatto, D., 2002. Zircon trace element geochemistry: partitioning with garnet and the link between U-Pb ages and metamorphism. Chemical Geology, 184, 123-138.

Rubatto, D., 2017. Zircon: the metamorphic mineral. Reviews in Mineralogy and Geochemistry, 83, in press.

Rubatto, D., Chakraborty, S., Dasgupta, S., 2013. Timescales of crustal melting in the Higher Himalayan Crystallines (Sikkim, Eastern Himalaya) inferred from trace element-constrained monazite and zircon chronology. Contributions to Mineralogy and Petrology, 165, 349-372.

Rubatto, D., Hermann, J., Berger, A., Engi, M., 2009. Protracted fluid-induced melting during Barrovian metamorphism in the Central Alps. Contributions to Mineralogy and Petrology, 158, 703-722.

Rubatto, D., Regis, D., Hermann, J., Boston, K., Engi, M., Beltrando, M., McAlpine, S.R.B., 2011. Yo-yo subduction recorded by accessory minerals in the Italian Western Alps. Nature Geoscience, 4, 338-342.

Rütti, R., Marquer, D., Thompson, A.B., 2008. Tertiary tectono-metamorphic evolution of the European margin during Alpine collision: example of the Leventina Nappe (Central Alps, Switzerland). Swiss Journal of Geoscience, 101, S157-S171.

Schlunegger, F., 1999. Controls of surface erosion on the evolution of the Alps:

constraints from the stratigraphies of the adjacent foreland basins. International Journal of Earth Sciences, 88, 285-304

Schmid, S., Aebli, H.R., Heller, F., Zingg, A., 1989. The role of the Periadriatic Line in the tectonic evolution of the Alps. In M.P. Coward, D. Dietrich, R.G. Park (Eds.), Conference on Alpine tectonics. Geological Society Special Publications, 45, 153-171.

Shaw, D.M., 1956. Geochemistry of pelitic rocks. Part III: major elements and general geochemistry. Geological Society of America Bulletin, 67, 919-934.

Smith, H.A., Barreiro, B., 1990. Monazite U-Pb dating of staurolite grade metamorphism in pelitic schists. Constributions to Mineralogy and Petrology, 105, 602-615.

Smye, A.J., Roberts, N.M.W., Condon, D.J., Horstwood, M.S.A., Parrish, R.R., 2014. Characterising the U-Th-Pb systematics of allanite by ID and LA-ICPMS: Implications for geochronology. Geochimica et Cosmochimica Acta, 135, 1-28.

Spear, F.S., 2010. Monazite–allanite phase relations in metapelites. Chemical Geology, 279, 55-62.

Spear, F.S., Pyle, J.M., 2010. Theoretical modelling of monazite growth in a low-Ca metapelite. Chemical Geology, 273, 111-119.

Stacey, J.S., Kramers, J.D., 1975. Approximation of terrestrial lead isotope evolution by a two-stage model. Earth and Planetary Science Letters, 26, 207-221.

Steck, A., Della Torre, F., Keller, H., Pfeifer, H.-R., Hunziker, J., Masson, H., 2013. Tectonics of the Lepontine Alps: Ductile thrusting and folding in the deepest tectonic levels of the Central Alps. Swiss Journal of Geosciences, 106, 427-450.

Steck, A., Hunziker, J., 1994. The Tertiary structural and thermal evolution of the Central Alps – compressional and extensional structures in an orogenic belt. Tectonophysics, 238, 229-254.

Todd, C.S., Engi, M., 1997. Metamorphic field gradients in the Central Alps. Journal of metamorphic Geology, 15, 513-530.

Trommsdorff, V., 1980. V. General questions. 1. Alpine metamorphism and Alpine intrusions. In R. Trümpy (Ed.), Geology of Switzerland: a guide book. Part A: An outline of the Geology of Switzerland (pp. 82-87). Basel: Wepf & Co.

Trommsdorff, V., Hermann, J., Müntener, O., Pfiffner, M., Risold, A.-C., 2000. Geodynamic cycles of subcontinental lithosphere in the Central Alps and the Arami enigma. Journal of Geodynamics, 30, 77-92.

Vance, D., O'Nions, R.K, 1992. Prograde and retrograde thermal histories from the central Swiss Alps. Earth and Planetary Science Letters, 114, 113-129.

von Blanckenburg, F., 1992. Combined high-precision chronometry and geochemical tracing using accessory minerals: applied to the Central-Alpine Bergell intrusion (central Europe). Chemical Geology, 100, 19-40.

Vonlanthen, P., Fitz Gerald, J.D., Rubatto, D., Hermann, J., 2012. Recrystallization rims in zircon (Valle d'Arbedo, Switzerland): An integrated cathodoluminescence, LA-ICP-MS, SHRIMP, and TEM study. American Mineralogist, 97, 369-377.

Vry, J.K. Baker, J.A., 2006. LA-MC-ICPMS Pb–Pb dating of rutile from slowly cooled granulites: Confirmation of the high closure temperature for Pb diffusion in rutile. Geochimica et Cosmochimica Acta 70, 1807-1820.

Wang, J.-M., Rubatto, D., Zhang, J.-J., 2015. Timing of partial melting and cooling across the Greater Himalayan Crystalline Complex (Nyalam, central Himalaya): in-sequence thrusting and its implications. Journal of Petrology, 56, 1677-1702.

Warren, C. J., Grujic, D., Cottle, J. M., Rogers, N. W., 2012. Constraining cooling histories: rutile and titanite chronology and diffusion modelling in NW Bhutan. Journal of Metamorphic Geology, 30, 113-130.

Wiederkehr, M., Bousquet, R., Schmid, S.M., Berger, A., 2008. From subduction to collision: thermal overprint of HP/LT meta-sediments in the north-eastern Lepontine Dome (Swiss Alps) and consequences regarding the tectono-metamorphic evolution of the Alpine orogenic wedge. Swiss Journal of Geoscience, 101, S127-155.

Wiederkehr, M., Sudo, M., Bousquet, R., Berger, A., Schmid, S.M., 2009. Alpine orogenic evolution from subduction to collisional thermal overprint: The $^{40}Ar/^{39}Ar$ age constraints from the Valaisan Ocean, central Alps. Tectonics, 28, TC6009.

Wiederkehr, M., Bousquet, R., Ziemann, M. A., Berger, A., Schmid, S., 2011. 3-D assessment of peak-metamorphic conditions by Raman spectroscopy of carbonaceous material: an example from the margin of the Lepontine dome (Swiss Central Alps). International Journal of Earth Sciences, 100, 1029-1063.

Wing, B.A., Ferry, J.M., Harrison, T.M., 2003. Prograde destruction and formation of monazite and allanite during contact and regional metamorphism of pelites: petrology and geochronology. Contributions to Mineralogy and Petrology 145, 228-250.

Table 1: Sample overview showing the main and accessory mineral assemblage, the minerals used for dating and the results of U-Th-Pb geochronology.

	Swiss Grid coordinates				Mineral assemblage			
Sample	X	Y	Location	Rock type	Main	Accessory	Mineral dated	Age (Ma)
Ma9330[1]	666.51	124.88	Croveo, (N of Domodossola)	Metapelite	Qtz Wm Bt Pl Grt St Ky	Mnz Ap R Ilm Zrn	Mnz	21.7 ± 0.4
Ba0903A	682.20	143.37	Robiei	Metapelite "Bündnerschiefer"	Qtz, Wm Bt Pl Grt Cal	Aln Rt Ilm Zrn	Rt	(21–27)[3]
Ba0901	683.23	142.70	Robiei	Gneiss	Qtz Wm Bt Kfs Pl	Aln Ap Zrn Rt	Aln cores Aln rims	26.8 ± 1.3 19.7 ± 1.3
CLB-3	697.37	147.60	Campolungo	Metapelite "Bündnerschiefer"	Qtz Wm Bt Pl Grt	Aln Rt Zrr	Aln	31.7 ± 1.1
CLB-4	697.37	147.60	Campolungo	Metapelite "Bündnerschiefer"	Qtz Wm Bt Pl Grt Ky St	Aln Rt Zrn	Rt	(19–25)[3]
CLM-5	698.04	146.94	Campolungo	Metasediment, basement	Qtz Wm Bt Pl Grt St Ky	Zrn Mnz Tur	Mnz	332 ± 4
CLM-6	698.82	146.66	Campolungo	Metasediment, basement	Qtz Wm Bt Pl Grt St	Zrn Mnz	Mnz	326 ± 4
Ma0901	698.29	147.23	Campolungo	Metaquartzite	Qtz Wm Bt Pl Grt	Ap Aln Rt Zrn	Aln	28.5 ± 1.3
Sp9712	702.78	142.20	Alpe Sponda	Metasediment, basement	Qtz Wm Bt Pl Grt St Ky	Mnz Rt Zr	Mnz Rt	22.0 ± 0.4 (57–33)[3]
LEP0979[2]	743.95	130.70	Forcola	Orthogneiss	Qtz Wm t Kfs Pl	Aln Zrn	Aln	25–31
LEP0980[2]	744.05	131.24	Forcola	Orthogneiss	Qtz Wm Bt Chl Kfs Pl	Aln Zrn	Mosaic Aln Regular Aln	31.3 ± 1.1 27–31
LEP0807[2]	744.18	131.38	Forcola	Orthogneiss	Qtz Wm Bt Chl Kfs Pl	Aln Zrn	Aln	27.4 ± 0.6

[1] Ma9330 is the sample used in Todd & Engi, 1997

[2] LEP0807, -0979 and -0980 were donated by C Augenstein

[3]These are not formation ages, but dates that may include inheritance and Pb loss after formation, see text for discussion.

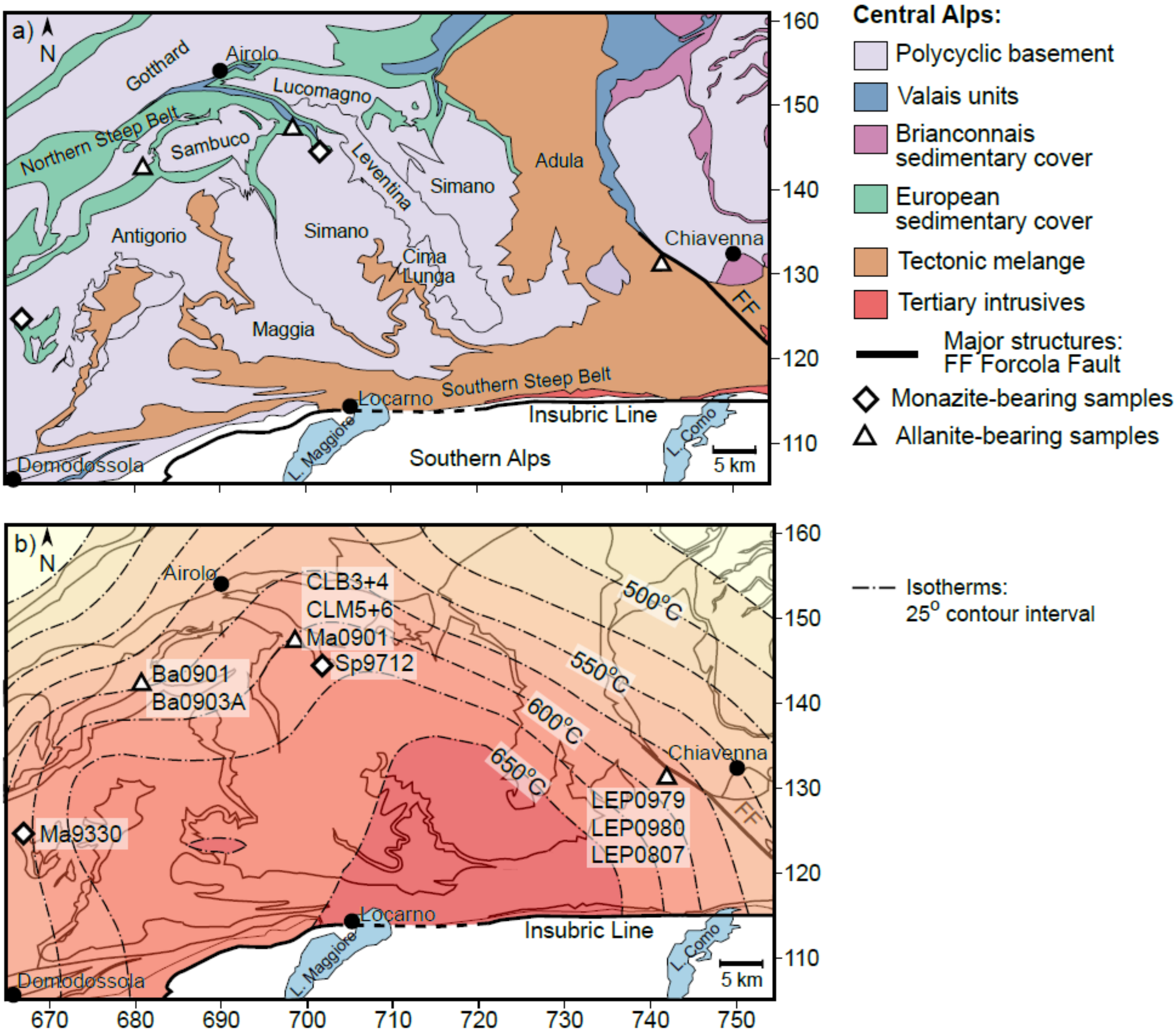
a)
N
Gotthard
Airolo
Lucomagno
Northern Steep Belt
Sambuco
Leventina
Simano
Adula
Antigorio
Simano
Chiavenna
Cima
Lunga
FF
Maggia
Southern Steep Belt
Locarno
Insubric Line
L. Maggiore
L. Como
Southern Alps
Domodossola
5 km
160
150
140
130
120
110
Central Alps:
Polycyclic basement
Valais units
Brianconnais sedimentary cover
European sedimentary cover
Tectonic melange
Tertiary intrusives
Major structures:
FF Forcola Fault
Monazite-bearing samples
Allanite-bearing samples
b)
N
Airolo
CLB3+4
CLM5+6
Ma0901
Sp9712
Ba0901
Ba0903A
500°C
550°C
600°C
650°C
Chiavenna
LEP0979
LEP0980
LEP0807
FF
Ma9330
Locarno
Insubric Line
L. Maggiore
L. Como
Domodossola
5 km
670
680
690
700
710
720
730
740
750
Isotherms:
25° contour interval

Figure 1

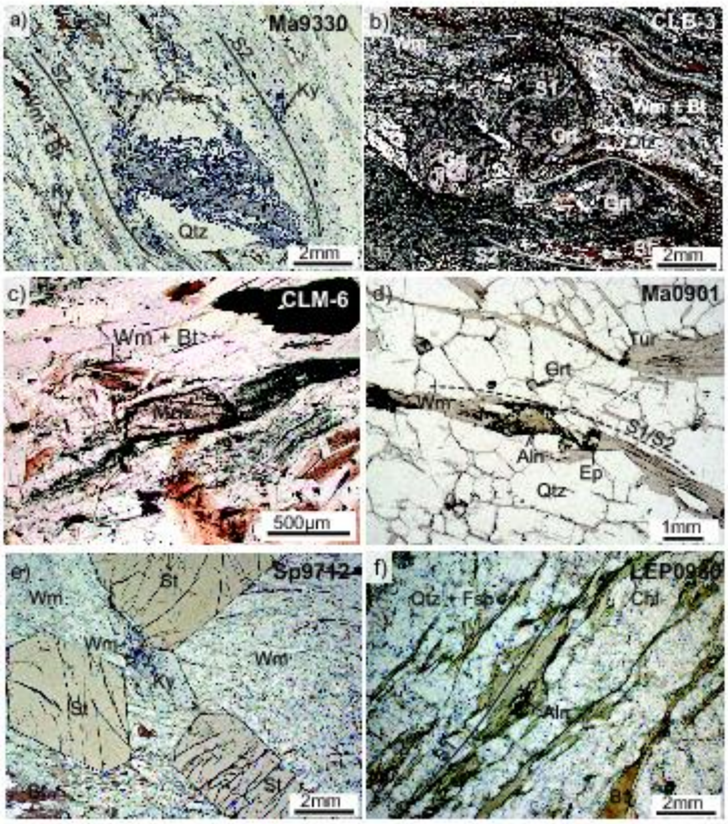
a)
Ma9330
Ky
Qtz
2mm
b)
CLB-3
Wm + Bt
S1
Grt
2mm
c)
CLM-6
Wm + Bt
500μm
d)
Ma0901
Tur
Grt
Wm
S1/S2
Aln
Ep
Qtz
1mm
e)
Sp9742
Wm
St
Ky
2mm
f)
Chl
Aln
Bt
2mm

Figure 2

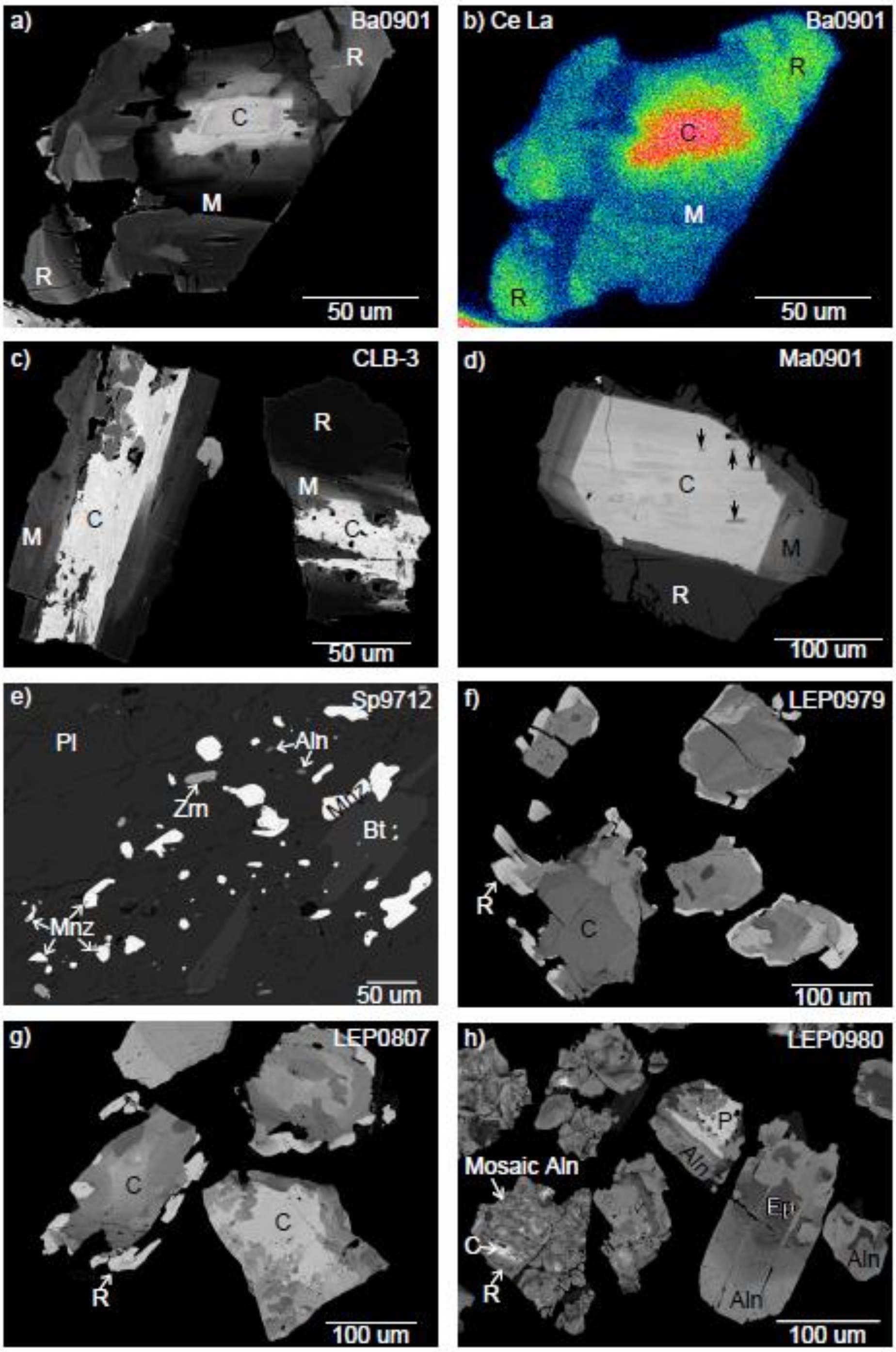
a)
Ba0901
R
C
M
R
50 um
b) Ce La
Ba0901
R
C
M
R
50 um
c)
CLB-3
R
M
C
M
C
50 um
d)
Ma0901
C
M
R
100 um
e)
Sp9712
Pl
Aln
Zrn
Mnz
Bt
Mnz
50 um
f)
LEP0979
R
C
100 um
g)
LEP0807
C
C
R
100 um
h)
LEP0980
P
Aln
Mosaic Aln
Ep
C
R
Aln
Aln
100 um

Figure 3

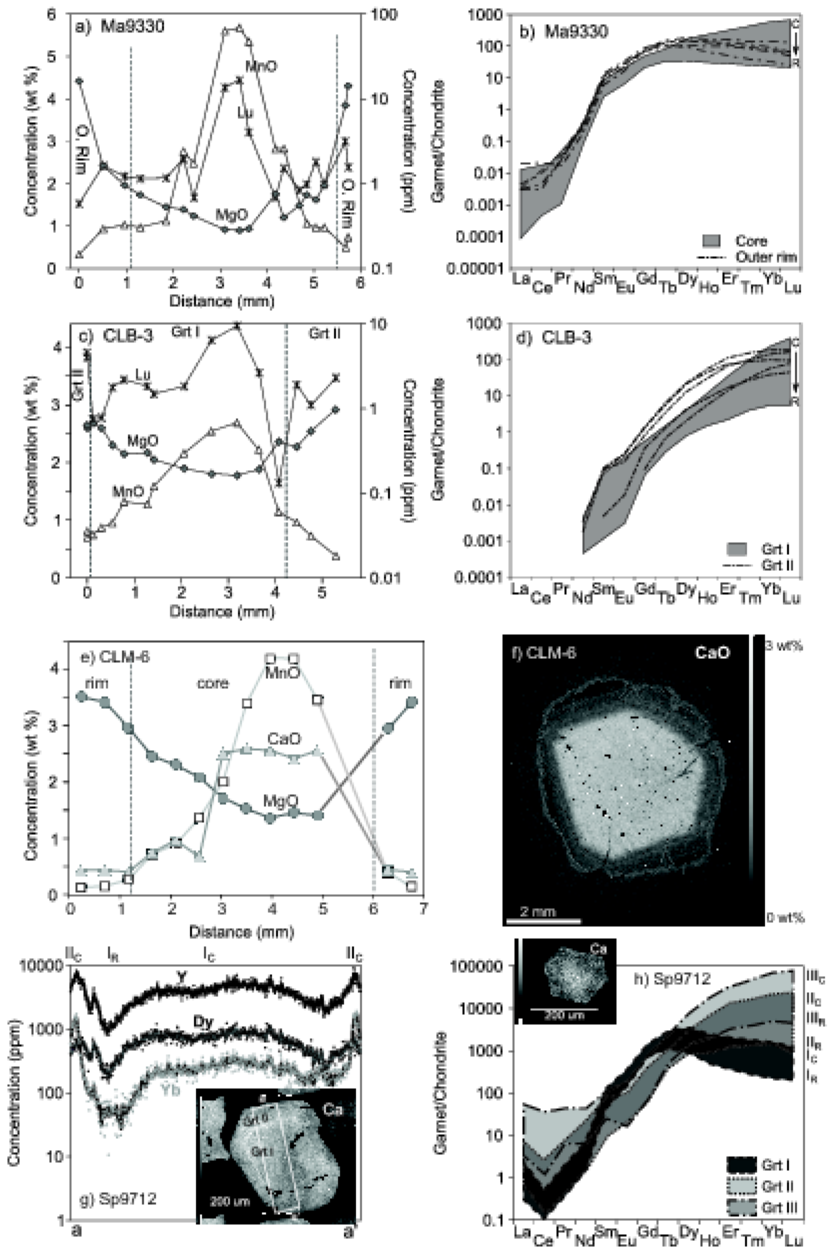
a) Ma9330
b) Ma9330
c) CLB-3
d) CLB-3
e) CLM-6
f) CLM-6
CaO
g) Sp9712
h) Sp9712
Concentration (wt %)
Concentration (ppm)
Distance (mm)
Garnet/Chondrite
MnO
Lu
MgO
CaO
O. Rim
Core
Outer rim
Grt I
Grt II
Grt III
rim
core
Y
Dy
Yb
Ca
2 mm
200 um
3 wt%
0 wt%
La
Ce
Pr
Nd
Sm
Eu
Gd
Tb
Dy
Ho
Er
Tm
Yb
Lu

Figure 4

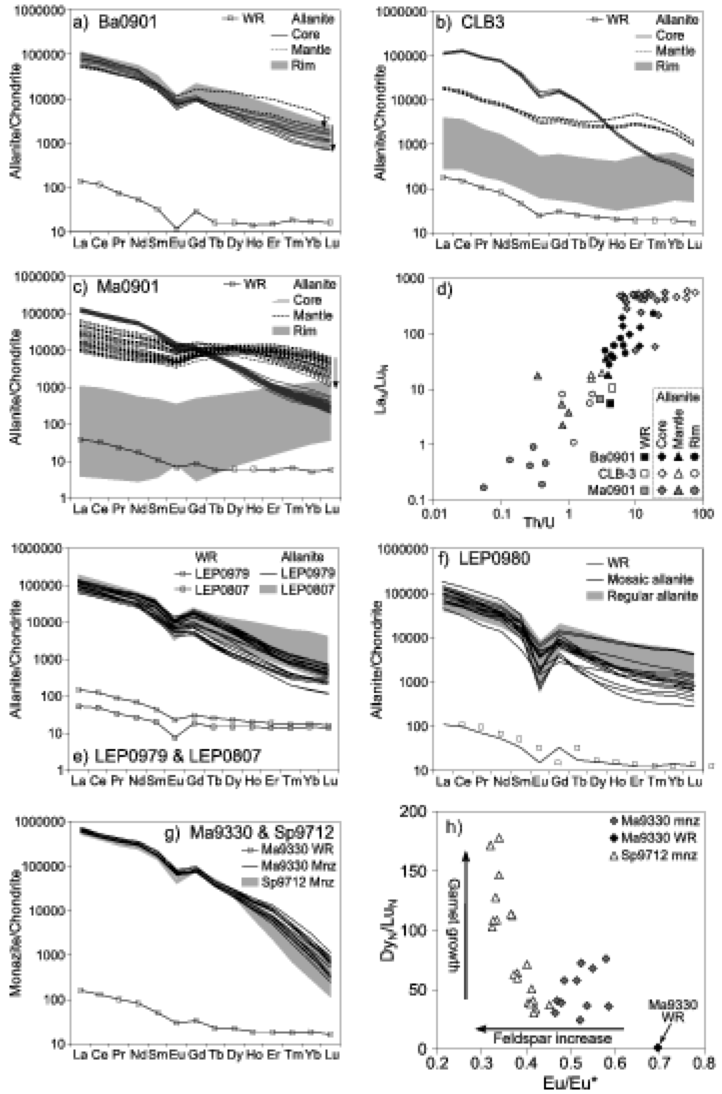
a) Ba0901
b) CLB3
c) Ma0901
d)
e) LEP0979 & LEP0807
f) LEP0980
g) Ma9330 & Sp9712
h)
Allanite/Chondrite
Monazite/Chondrite
WR
Allanite
Core
Mantle
Rim
Mosaic allanite
Regular allanite
Ma9330 WR
Ma9330 Mnz
Sp9712 Mnz
Ma9330 mnz
Sp9712 mnz
Th/U
Eu/Eu*
Garnet growth
Feldspar increase
La Ce Pr Nd Sm Eu Gd Tb Dy Ho Er Tm Yb Lu

Figure 5

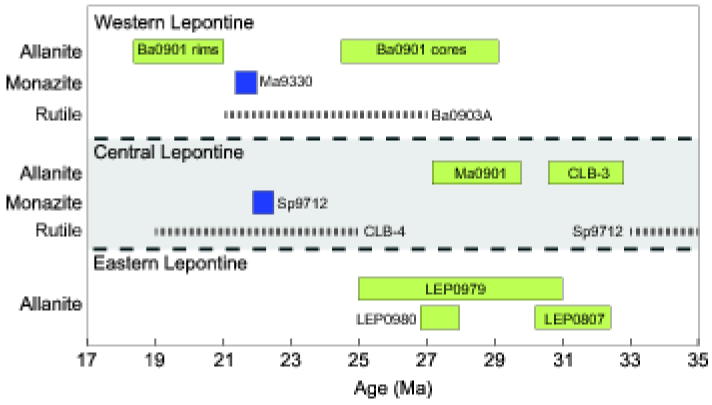
Western Lepontine
Allanite
Monazite
Rutile
Ba0901 rims
Ba0901 cores
Ma9330
Ba0903A
Central Lepontine
Allanite
Monazite
Rutile
Ma0901
CLB-3
Sp9712
CLB-4
Sp9712
Eastern Lepontine
Allanite
LEP0979
LEP0980
LEP0807
17
19
21
23
25
27
29
31
33
35
Age (Ma)

Figure 6

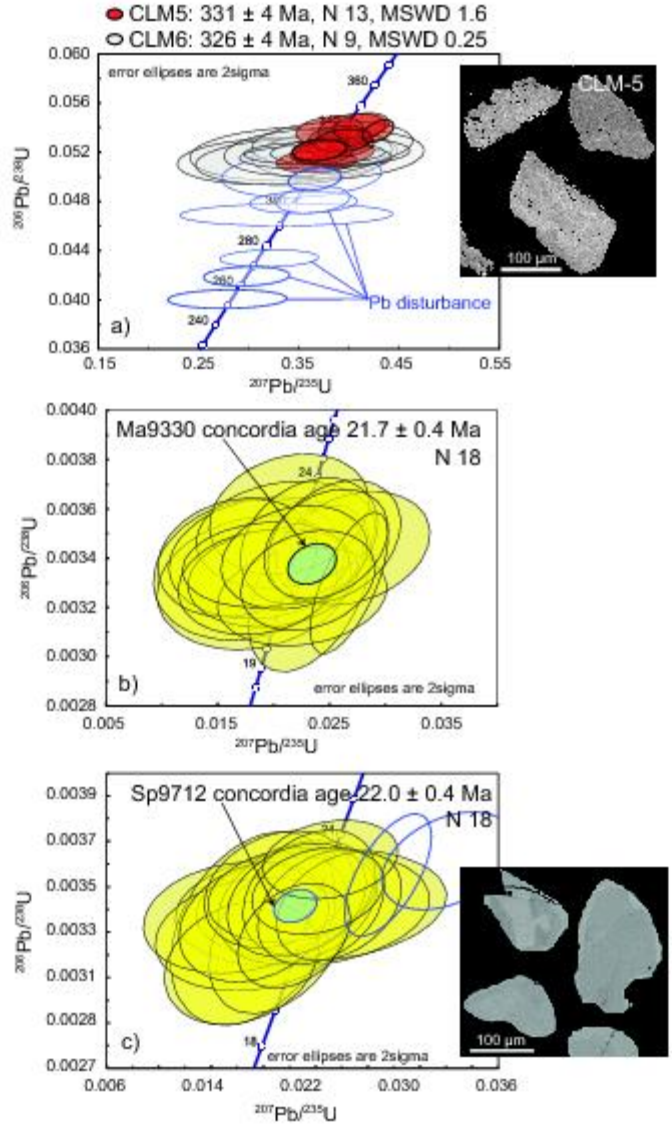

CLM5: 331 ± 4 Ma, N 13, MSWD 1.6
CLM6: 326 ± 4 Ma, N 9, MSWD 0.25
error ellipses are 2sigma
CLM-5
100 µm
Pb disturbance
a)
$^{206}Pb/^{238}U$
$^{207}Pb/^{235}U$
Ma9330 concordia age 21.7 ± 0.4 Ma
N 18
b)
error ellipses are 2sigma
$^{206}Pb/^{238}U$
$^{207}Pb/^{235}U$
Sp9712 concordia age 22.0 ± 0.4 Ma
N 18
c)
error ellipses are 2sigma
100 µm
$^{206}Pb/^{238}U$
$^{207}Pb/^{235}U$

Figure 7

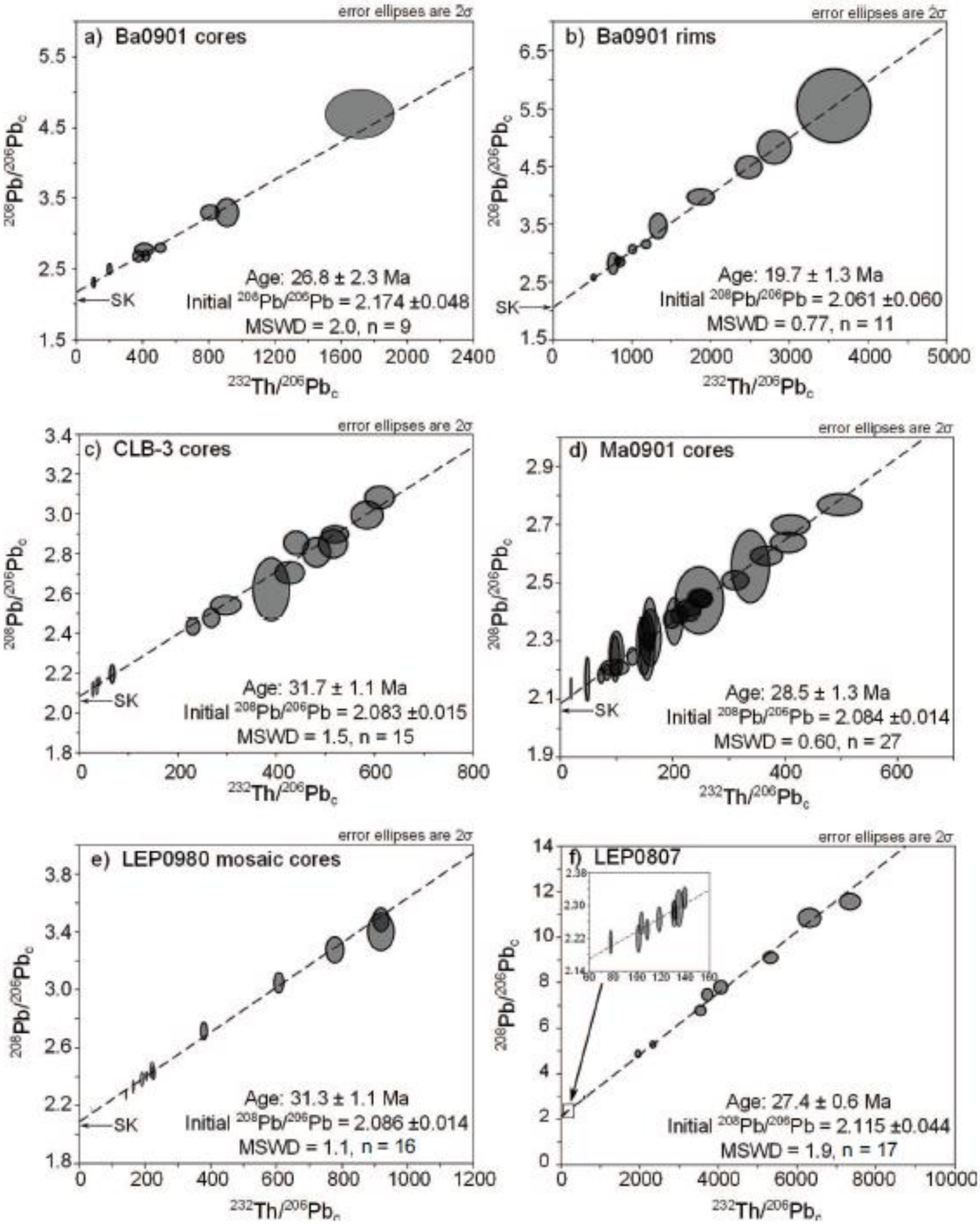
error ellipses are 2σ
a) Ba0901 cores
Age: 26.8 ± 2.3 Ma
Initial 208Pb/206Pb = 2.174 ±0.048
MSWD = 2.0, n = 9
SK
b) Ba0901 rims
Age: 19.7 ± 1.3 Ma
Initial 208Pb/206Pb = 2.061 ±0.060
MSWD = 0.77, n = 11
c) CLB-3 cores
Age: 31.7 ± 1.1 Ma
Initial 208Pb/206Pb = 2.083 ±0.015
MSWD = 1.5, n = 15
d) Ma0901 cores
Age: 28.5 ± 1.3 Ma
Initial 208Pb/206Pb = 2.084 ±0.014
MSWD = 0.60, n = 27
e) LEP0980 mosaic cores
Age: 31.3 ± 1.1 Ma
Initial 208Pb/206Pb = 2.086 ±0.014
MSWD = 1.1, n = 16
f) LEP0807
Age: 27.4 ± 0.6 Ma
Initial 208Pb/206Pb = 2.115 ±0.044
MSWD = 1.9, n = 17
208Pb/206Pbc
232Th/206Pbc

Figure 8

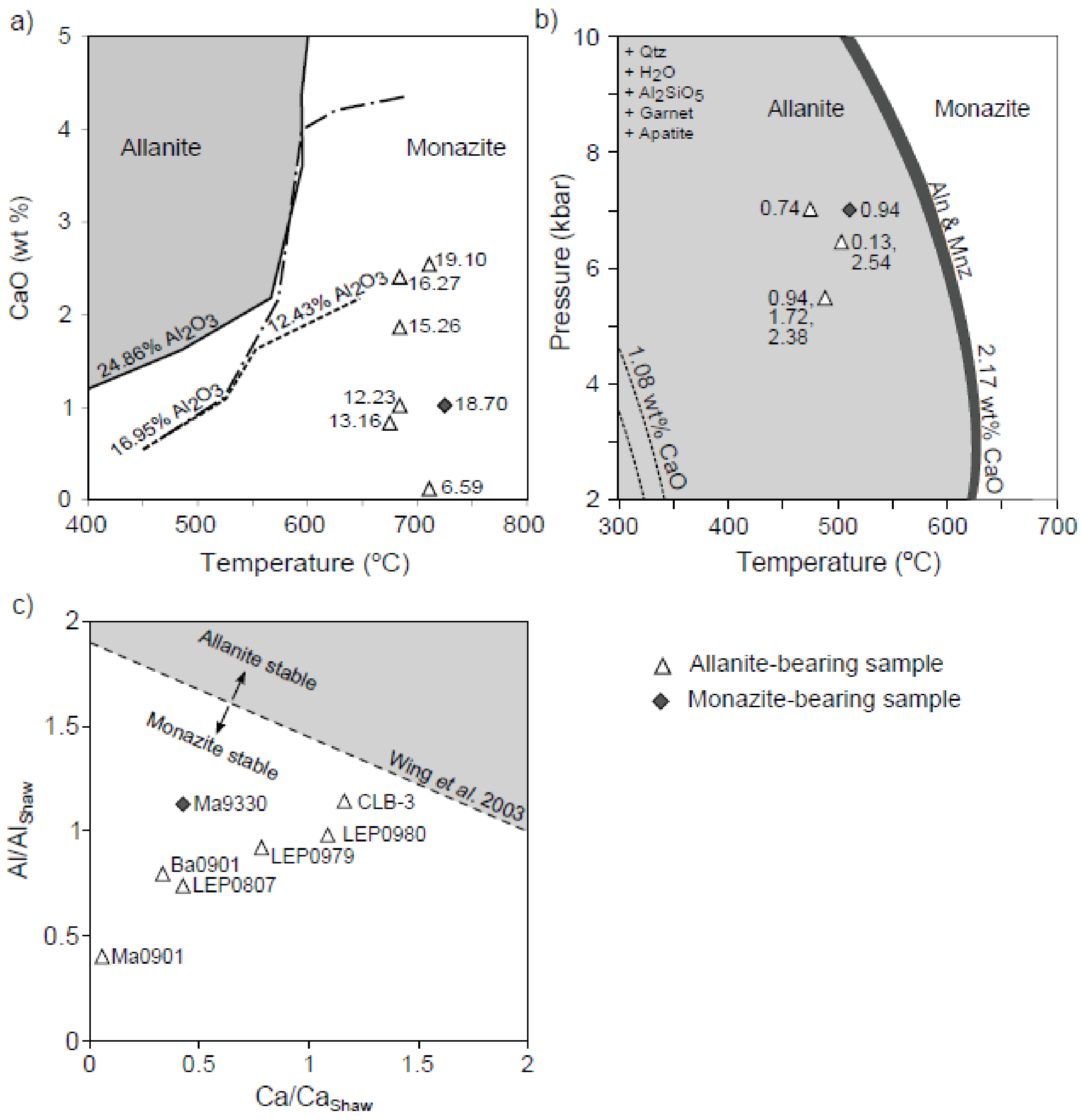

a)
Allanite
Monazite
CaO (wt %)
Temperature (°C)
24.86% Al2O3
16.95% Al2O3
12.43% Al2O3
19.10
16.27
15.26
12.23
13.16
18.70
6.59
b)
+ Qtz
+ H2O
+ Al2SiO5
+ Garnet
+ Apatite
Allanite
Monazite
Aln & Mnz
Pressure (kbar)
Temperature (°C)
0.74
0.94
0.13,
2.54
0.94,
1.72,
2.38
1.08 wt% CaO
2.17 wt% CaO
c)
Allanite stable
Monazite stable
Wing et al. 2003
Ma9330
CLB-3
LEP0980
LEP0979
Ba0901
LEP0807
Ma0901
Al/Al_Shaw
Ca/Ca_Shaw
Allanite-bearing sample
Monazite-bearing sample

Figure 9

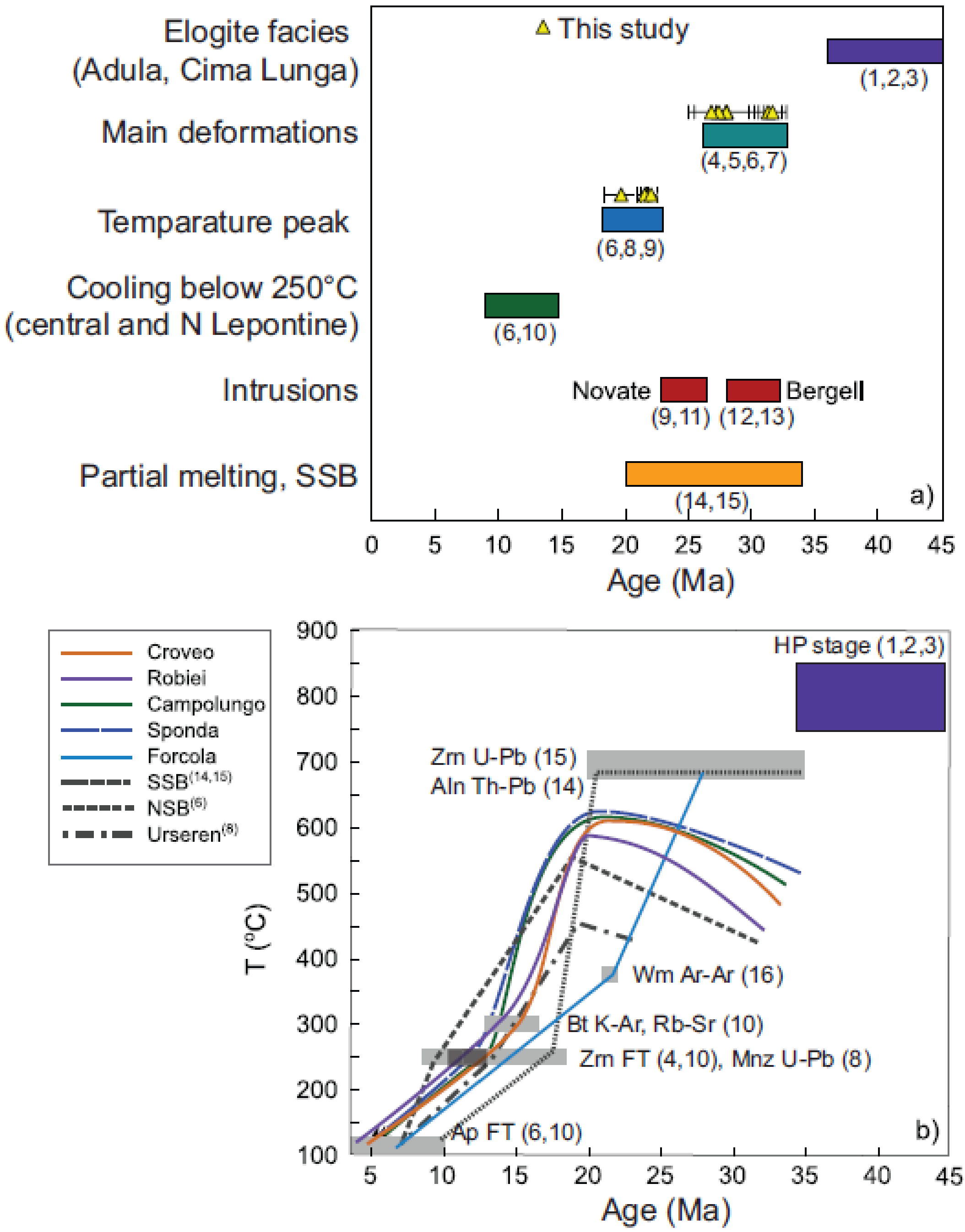

This study
Elogite facies
(Adula, Cima Lunga)
(1,2,3)
Main deformations
(4,5,6,7)
Temparature peak
(6,8,9)
Cooling below 250°C
(central and N Lepontine)
(6,10)
Intrusions
Novate
Bergell
(9,11) (12,13)
Partial melting, SSB
(14,15)
a)
0 5 10 15 20 25 30 35 40 45
Age (Ma)
Croveo
Robiei
Campolungo
Sponda
Forcola
SSB(14,15)
NSB(6)
Urseren(8)
HP stage (1,2,3)
Zrn U-Pb (15)
Aln Th-Pb (14)
Wm Ar-Ar (16)
Bt K-Ar, Rb-Sr (10)
Zrn FT (4,10), Mnz U-Pb (8)
Ap FT (6,10)
b)
T (°C)
900 800 700 600 500 400 300 200 100
5 10 15 20 25 30 35 40 45
Age (Ma)

Figure 10

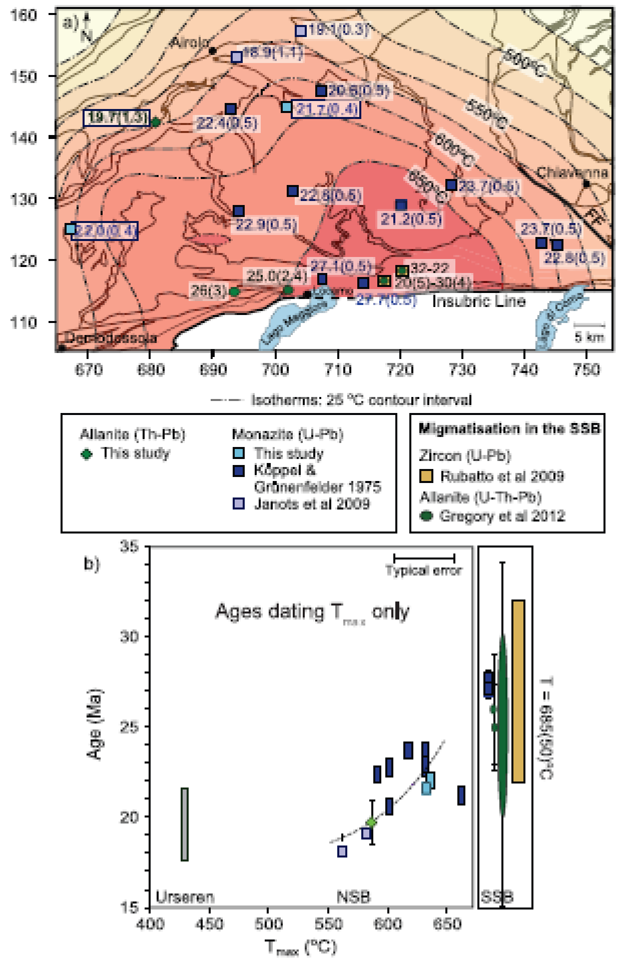
a)
N
Airolo
Chiavenna
Domodossola
Locarno
Lago Maggiore
Lago di Como
Insubric Line
FF
5 km
500°C
550°C
600°C
650°C
19.1(0.3)
18.9(1.1)
20.8(0.5)
21.7(0.4)
22.4(0.5)
19.7(1.3)
22.8(0.5)
23.7(0.5)
21.2(0.5)
22.9(0.5)
22.0(0.4)
23.7(0.5)
22.8(0.5)
27.1(0.5)
25.0(2.4)
26(3)
32-22
20(5)-30(4)
27.7(0.5)
160
150
140
130
120
110
670
680
690
700
710
720
730
740
750
Isotherms: 25 °C contour interval
Allanite (Th-Pb)
This study
Monazite (U-Pb)
This study
Köppel & Grünenfelder 1975
Janots et al 2009
Migmatisation in the SSB
Zircon (U-Pb)
Rubatto et al 2009
Allanite (U-Th-Pb)
Gregory et al 2012
b)
Typical error
Ages dating T_{max} only
Age (Ma)
35
30
25
20
15
Urseren
NSB
SSB
T = 685(50)°C
400
450
500
550
600
650
T_{max} (°C)

Figure 11

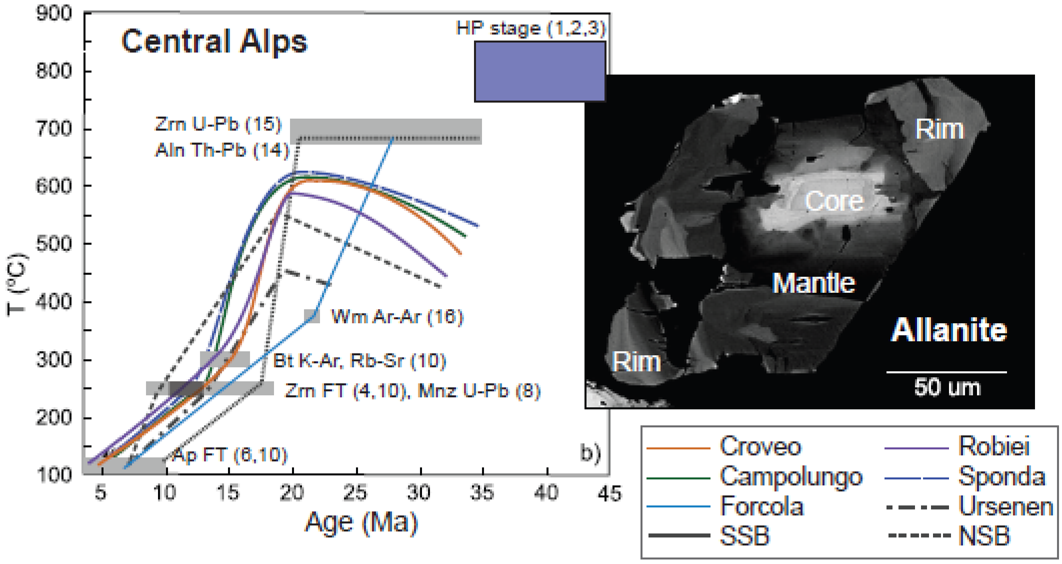

Graphical abstract

Highlights

Ages of allanite, monazite and rutile in amphibolite facies rocks across the Barrovian sequence of the Central Alps (Switzerland) record different stages of metamorphism.

In situ U-Th-Pb dating of allanite and monazite by SHRIMP ion microprobe revealed systematic trends for the ages of Alpine main deformation and temperature in the Lepontine dome.

Prograde allanite records ages between ~32 and 27 Ma from East to West related to the main deformation event.

The thermal peak is dated at ~ 22 Ma by monazite that grew at the expenses of allanite in the central and western region.

A Variscan metamorphic age of ~ 330 Ma is recorded in monazite of the central Lepontine.

The results imply that fast cooling of the Lepontine nappe was related to tectonic exhumation.